nature communications

Article

https://doi.org/10.1038/s41467-025-60374-4

Translation suppresses exogenous target RNA-mediated microRNA decay

Received: 29 April 2024

Accepted: 21 May 2025

Published online: 06 June 2025

Check for updates

Tianqi Li[1,2,3], Lu Li[1,2], Nicholas M. Hiers[1,2], Peike Sheng[1,2], Yuzhi Wang[1,2], Conner M. Traugot[1,4], Jessi F. Effinger-Morris[1], Pitchaporn Akaphan[1,5,6], Yanyan Liu[1,2], Jiang Bian[2,7], Kotaro Fujii[4,5,6] & Mingyi Xie[1,2,4]

MicroRNAs (miRNAs) interact with the target mRNAs to induce translational repression and mRNA degradation. Interestingly, miRNAs themselves can turnover rapidly when binding to a target RNA with extensive complementarity, a phenomenon called target-directed miRNA degradation (TDMD). To date, all validated TDMD "triggers" can induce miRNA degradation reside in non-coding regions of the RNA. We found that TDMD triggers placed in the 3′ untranslated region (UTR) of a reporter degraded miRNAs more effectively than those in the coding sequence (CDS). Inhibiting translation of the reporter enhanced miRNA degradation by the CDS trigger, indicating that ribosome-free CDS triggers are more accessible to miRNAs. By small RNA sequencing, we explored mammalian miRNAs sensitive to global translation status. Yet, no endogenous CDS trigger could be confidently assigned to these miRNAs. Our work revealed the intricate relationship between translation and TDMD, and explains the paucity of effective TDMD triggers in the CDS.

MicroRNAs (miRNAs) are a class of endogenous ~22 nucleotide (nt) non-coding RNAs (ncRNAs). Canonically, AGO-bound miRNAs primarily interact with target mRNAs through the seed region (nt 2–8 from the miRNA 5′ end) to recruit factors that facilitate translational repression[1]. Ultimately, miRNA binding leads to target mRNA deadenylation, decapping and degradation. Despite the extensive knowledge regarding miRNA biogenesis and functions, our understanding of miRNA decay remains relatively limited. In general, miRNAs are quite stable in vivo when associating with AGO, with half-lives extending up to several days[2–9]. This is because miRNAs are sheltered within AGO, protecting them from ribonucleases[10]. However, it is noteworthy that a minority of miRNAs display a degree of instability, characterized by relatively short half-lives, often within a few hours[2–9].

For many short-lived miRNAs, this instability arises from extensive base-pairing of the 3′ end of miRNA in addition to seed region base-pairing with the target RNAs. Such a mode of interaction induces rapid miRNA degradation, a phenomenon called "target-directed miRNA degradation" (TDMD)[11–22]. In 2020, the Bartel and Mendell groups identified a Cullin-RING E3 ubiquitin ligase complex component, ZSWIM8, that plays a role in most TDMD events, presumably by recognizing an AGO conformation specifically associated with TDMD[23,24]. This recognition leads to the polyubiquitylation and subsequent proteasomal decay of AGO, exposing the miRNA to ribonucleases, resulting in miRNA decay. Knock out of ZSWIM8 or its ortholog in *C. elegans*[25], *Drosophila*[12,18], mice[23,24,26,27] and various human cell lines[23,24] led to an increase in about 100 miRNAs, referred to as "ZSWIM8-sensitive" miRNAs, suggesting that TDMD is a conserved mechanism across metazoans.

In contrast to the large number of miRNAs under TDMD control, there are only a few known endogenous transcripts, also known as TDMD "triggers", that can form extensive base-pairing with certain miRNAs and induce their degradation. While some predicted triggers localize to mRNA coding sequences, validated endogenous TDMD triggers in both vertebrates and *Drosophila melanogaster* are in the

[1]Department of Biochemistry and Molecular Biology, University of Florida, Gainesville, FL 32610, USA. [2]UF Health Cancer Center, University of Florida, Gainesville, FL 32610, USA. [3]Department of Pharmacology, University of California San Diego, La Jolla, CA, USA. [4]UF Genetics Institute, University of Florida, Gainesville, FL 32610, USA. [5]Department of Molecular Genetics and Microbiology, University of Florida, Gainesville, FL 32610, USA. [6]Center for NeuroGenetics, University of Florida, Gainesville, FL 32610, USA. [7]Department of Health Outcomes & Biomedical Informatics, University of Florida, Gainesville, FL 32610, USA. e-mail: mingyi.xie@ufl.edu

https://doi.org/10.1038/s41467-025-60374-4

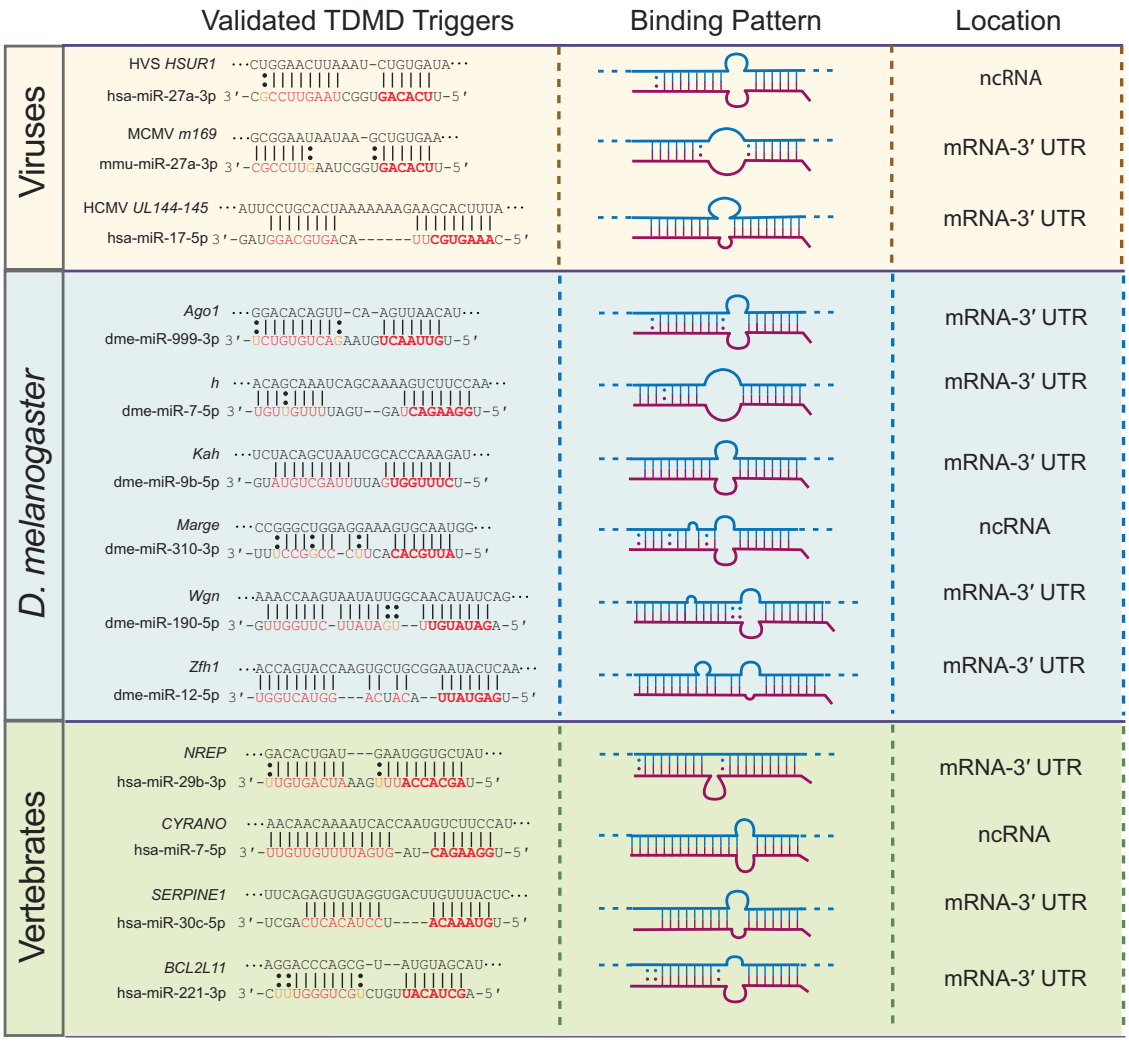

Fig. 1 | Validated endogenous TDMD triggers. A list of validated endogenous TDMD triggers, with their genetic origins[13], trigger-miRNA base pairing patterns, and the location of trigger sequences.

non-coding regions of RNA, suggesting that TDMD triggers may be more effective in the non-coding regions. Similarly, most of miRNA recognition sites for the miRNA-mediated gene repression are preferentially situated within the 3′ UTR of target mRNA[1]. Ribosome translocation on mRNA hinders the accessibility of the RNA-induced silencing complex (RISC) to the miRNA recognition sites, ranging from the translational initiation site to the stop codon, including the first ~15 nt of the 3′ UTR[28–30]. However, target sites that are perfectly complementary to artificial small interference RNAs (siRNA) function well within the coding region and thus seemingly unaffected by ribosome interference[31]. Given that translation can impede miRNA-mediated downregulation but not siRNAs, we questioned whether ribosome translocation could influence TDMD, which requires extensive base-pairing and presumably tight association between miRNAs and their triggers.

In this study, we compared the efficacy of a TDMD trigger placed either in the CDS or 3′ UTR and detected the inhibition of TDMD by the translation machinery. Additionally, we employed accurate quantification by sequencing (AQ-seq) and AGO cross-linking ligation and sequencing of miRNA-mRNA hybrids (AGO-CLASH) to identify the potential miRNAs controlled by endogenous CDS triggers upon induction of ribosome stalling in human embryonic kidney (HEK) 293 T cells and in a mouse striatal cell model of Huntington's Disease (HD) where translation is inhibited[32–35]. While we detected a few miRNAs sensitive to translation inhibition, no corresponding endogenous CDS trigger was confidently assigned to these miRNAs. Our findings establish the basis for the observed selection of TDMD triggers in the non-coding sequences and suggest a possible explanation for the role of translation in controlling cellular miRNA levels through TDMD.

Results

TDMD triggers preferentially localize to noncoding regions of RNA

The rapidly expanding field of ZSWIM8-dependent TDMD research is elucidating mechanisms that regulate miRNA stability in animals. The accurate identification of endogenous miRNA triggers responsible for inducing TDMD is a major effort in this field. Both our group and others have previously identified such endogenous TDMD triggers in various models[13,36]. Interestingly, the endogenous TDMD trigger sites identified thus far are exclusively located in ncRNA and the 3′ UTR of mRNA (Fig. 1). Several viral triggers can induce the decay of host-encoded microRNAs, such as *Herpesvirus saimiri* (HVS) *HSUR1*: miR-27a/b[19], murine cytomegalovirus (MCMV) *m169*: miR-27a/b[21], and human cytomegalovirus (HCMV) *UL144-145*: miR-17/miR-20a[22,37]. In *Drosophila melanogaster*, currently annotated triggers are in the 3′ UTR of mRNA and lncRNA, including *Ago1*: miR-999, *h*: miR-7, *Kah*: miR-9b, *Wgn*: miR-190, *Zfh1*: miR-12, and *Marge*: miR-310[12,18]. Similarly,

in mammalian cells, the lncRNA *CYRANO* induces miR-7 degradation, and the triggers for miR-29b, miR-30c, and miR-221/222 locate in the 3′ UTR of *NREP*, *SERPINE1*, and *BCL2L11*, respectively[11,14,16,17].

In *D. melanogaster*, knockout of its ZSWIM8 ortholog (Dora) leads to embryonic lethality[18,38]. Mice deficient in ZSWIM8 display several developmental anomalies, including reduced birth weight, cyanosis, and significantly stunted development of the cardiopulmonary system, culminating in perinatal lethality[26,27]. Simultaneous knockout of several TDMD-sensitive miRNAs partially rescues the lethality and developmental defect in Dora-KO flies and ZSWIM8-KO mice[18,27]. These findings underscore a vital link between TDMD and developmental processes, potentially paving the way for further research into related developmental abnormalities. While prior research has identified nearly 100 metazoan miRNAs as responsive to ZSWIM8 across a variety of cell lines and organisms, the discovery of endogenous TDMD triggers remains limited, with only 10 identified so far (Fig. 1). Given that all the known endogenous triggers localize to non-coding regions of RNAs, we hypothesized that triggers localizing to coding regions may be less efficacious. Thus, we aim to investigate the functional difference in the localization of triggers in non-coding or coding regions.

TDMD triggers in the noncoding regions are more efficient

To gain insight into how localization of trigger sites might impact TDMD efficacy, we first aimed to compare the efficacy of the *CYRANO* TDMD trigger against miR-7 placed in either the CDS or 3′ UTR of a superfolder (sf)GFP reporter, under the control of a tetracycline-inducible promoter. To facilitate direct comparison between the two reporters, we moved the location of the stop codon to ensure that the sequences of the reporters are minimally modified (Supplementary Fig. 1a). We also incorporated the evolutionarily conserved flanking region spanning the trigger sequence of *CYRANO* to facilitate the interaction between the TDMD trigger and miR-7 (Supplementary Fig. 1a)[11,17,39]. The flanking region of several TDMD triggers was shown to be critical for their ability to induce miRNA degradation, while the *CYRANO* trigger without a flanking region could induce miR-7 degradation[11]. Therefore, we additionally designed “short” constructs that only contain the 26 nt TDMD trigger sequence without the flanking regions (Supplementary Fig. 1b).

The inducible *CYRANO* triggers were stably incorporated in HEK293T cells with or without ZSWIM8 knockout (KO). After the addition of doxycycline (Dox) for 24 hours, the total RNA was harvested, and miR-7 levels were measured by northern blot (Supplementary Fig. 1c). We observed that the 3′ UTR trigger more efficiently induced miR-7 degradation than the CDS trigger (Supplementary Fig. 1c, compare lane 5 to lane 2). However, it was difficult to interpret the efficacy of the inducible *CYRANO* reporter because of interference by endogenous *CYRANO*, which both limited the abundance of miR-7 and caused miR-7 to increase following ZSWIM8 KO (Supplementary Fig. 1c).

We next modified the miR-7 trigger in *CYRANO* to base pair with miR-16, which is not regulated by TDMD in mammals (Fig. 2a and 2b)[17,24,26]. In response to trigger induction with Dox for 24 hours, the 3′ UTR trigger could efficiently induce miR-16 TDMD (Fig. 2c right, 2d, and Supplementary Fig. 2a and 2b). Despite the CDS trigger expression being more abundant compared to the 3′ UTR trigger (Fig. 2e), it induced less efficient miR-16 degradation, but induced tailing (non-templated nucleotide addition) and trimming efficiently (Fig. 2c). In contrast, the “short” miR-16 TDMD triggers, present either in the CDS or 3′ UTR, could not induce miR-16 degradation effectively (Supplementary Fig. 2c, 2d and 2e). Interestingly, although less efficiently, the WT *CYRANO* trigger could induce miR-7 degradation in the “short” reporter when present in the 3′ UTR (Supplementary Fig. 1c, short reporters, compare lanes 12 to lane 9). One factor that may contribute to the different outcomes observed for miR-7 and miR-16 degradation could be the number of the miRNA 3′ base-pairings. Endogenous *CYRANO*: miR-7 interaction contains extensive fourteen 3′ end base-pairings, whereas the artificial trigger/miR-16 contains twelve 3′ end base-pairings (Fig. 2b and Supplementary Fig. 1b). It is possible that extended 3′ end base-pairing is more effective in destabilizing miRNAs even without the native *CYRANO* sequences surrounding the trigger.

To confirm that the reduction of mature miR-16 was dependent on ZSWIM8-mediated TDMD, we employed CRISPR-Cas9 to knock out ZSWIM8 in HEK293T cells stably expressing the inducible sfGFP reporter. It has been established that ZSWIM8-mediated TDMD destabilizes targeted miRNAs, effectively reducing their half-lives[19,23,24]. As expected, miR-16 degradation induced by CDS and 3′ UTR triggers could be rescued to similar levels when ZSWIM8 is knocked out (Fig. 2f, top blot, compare lanes 11 and 12 to lanes 8 and 9, and 2 g). The increase in miR-7 indicates successful ZSWIM8 KO (Fig. 2f, middle blot, compare KO lanes to Scr lanes). Additionally, TIDE (tracking of indels by decomposition) analyses revealed that approximately 90% of the cells modified by CRISPR-Cas9 had mutations in ZSWIM8, further supporting the ZSWIM8-dependency of miR-16 degradation induced by our reporter (Supplementary Fig. 2f). To check if trigger abundance causes differential degradation, we performed RT-qPCR in scramble control and ZSWIM8 KO cells to detect the trigger transcripts. As expected, there was no significant difference in trigger expression when comparing control to ZSWIM8 KO (Fig. 2e). There was also no difference in sfGFP protein levels when comparing control to ZSWIM8 KO cells (Supplementary Figs. 1d and 2g). It is worth noting that the CDS reporter clearly showed lower protein levels that may be the result of sfGFP misfolding when additional amino acids were introduced by incorporating the *CYRANO* trigger flanking region. Indeed, when the cells were treated with proteasome inhibitor MG132 so that misfolded proteins could accumulate, we observed an increase in sfGFP protein level with the CDS trigger, which is now closer to the sfGFP produced from the 3′ UTR reporter (Supplementary Fig. 2h). Additionally, the translation efficiencies of both CDS trigger and 3′ UTR trigger transcripts appear to be comparable, as evidenced by their distribution in the monosome and polysome fractions, determined by ribosome profiling (Supplementary Fig. 2i and 2j).

To explain the different efficiencies observed for miR-16 degradation, RT-qPCR was performed on transcripts enriched from AGO immunoprecipitation (AGO-IP). This experiment revealed that more 3′ UTR triggers than CDS triggers interact with AGO (Fig. 2h), even though the 3′ UTR trigger was less abundant (Fig. 2i). Therefore, the efficacy of TDMD triggers in different regions may be determined by their association with AGO proteins.

Translational repression on CDS triggers increases miR-16 degradation

We hypothesized that translational machinery moving across the sfGFP RNA may be competing with the interaction between AGO/miR-16 and the CDS trigger. Therefore, we tested whether inhibiting translation of the sfGFP reporter would increase the efficacy of TDMD by the CDS trigger. Translation can be inhibited by morpholino oligomers, which are synthetic molecules that are structurally based on natural nucleic acids with no ionic charge[40]. They are capable of binding to mRNA transcripts through canonical Watson-Crick base pairing without causing degradation of the RNA. These characteristics make them useful for blocking the translation of mRNA[40]. We used a morpholino oligo targeting the first 25 nt of the coding sequence of the sfGFP reporter to block translation initiation (Fig. 3a and Supplementary Data 1). The morpholino oligo was able to repress the sfGFP protein expression when observed by western blot (Fig. 3b, compare lane 6 to lanes 4, 5). In contrast, the abundance of sfGFP transcripts was not affected by the introduction of morpholino oligos (Fig. 3c). We noticed that the inhibition of sfGFP translation could significantly enhance the TDMD efficacy induced by the CDS trigger, to the same degree as the 3′ UTR trigger (Fig. 3d and 3e, compare lane 3 to lanes 1, 2). As expected,

https://doi.org/10.1038/s41467-025-60374-4

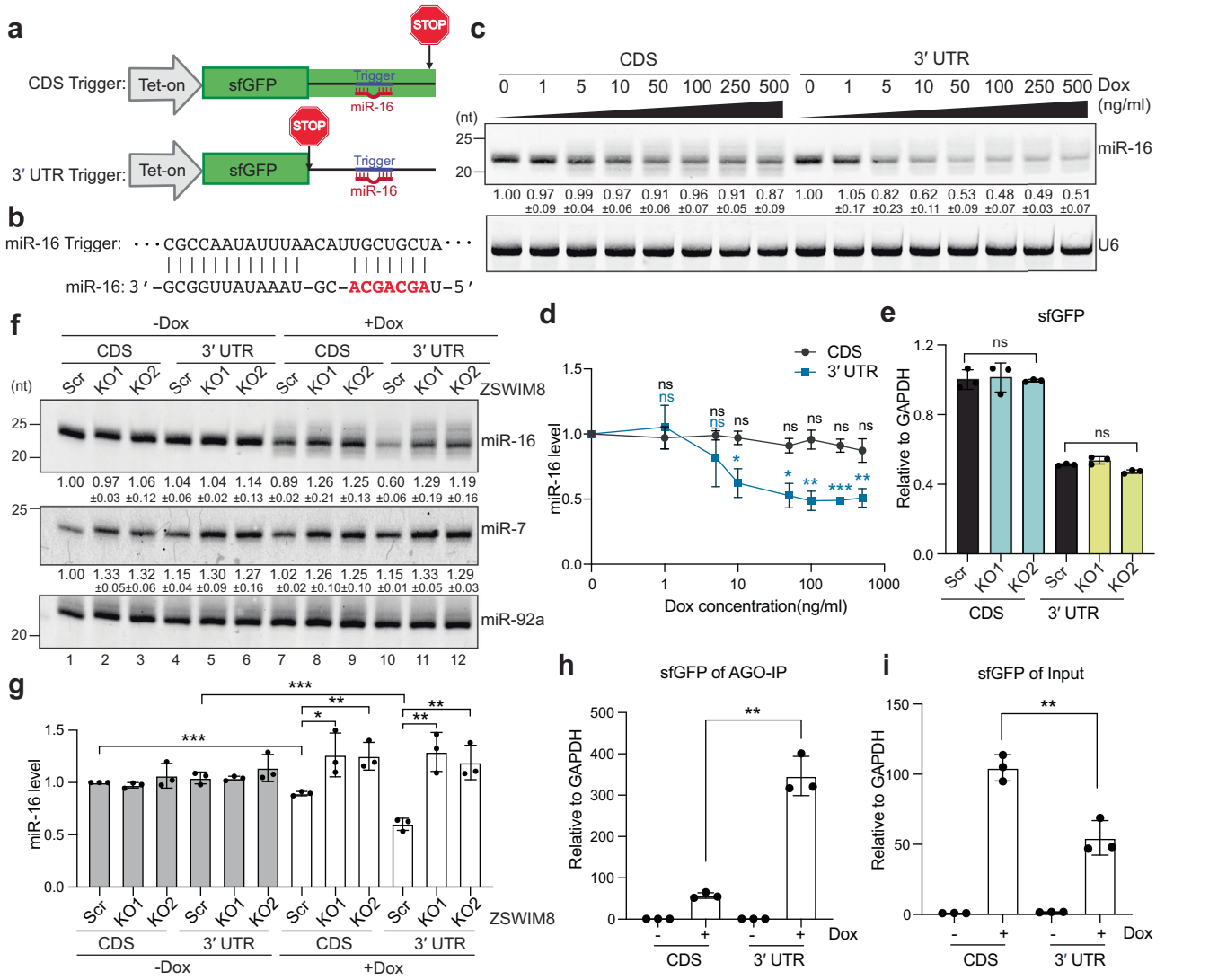

Fig. 2 | TDMD triggers preferably locate in the noncoding region of RNA transcripts. a Illustration of the inducible sfGFP reporter system containing an engineered trigger against miR-16. **b** Base-pairing pattern of miR-16 and its trigger, which mimics the pattern of *CYRANO*: miR-7. miR-16 seed region is highlighted in red. **c** Northern blot analyses of miR-16 in cells expressing inducible sfGFP reporters with the CDS or 3′ UTR trigger against miR-16. Cells were treated with different doses of Dox indicated above the blots. The normalized miRNA abundance and standard deviation are shown below each miRNA. miRNA abundance is normalized to U6. The miRNA abundance in CDS and 3′ UTR without Dox (0) treatment is normalized to 1, respectively. **d** The quantification of northern blots in **c**. miR-16 levels are normalized to U6 RNA and the value in cells without Dox treatment is set to 1. p(3′ UTR 10) = 0.0271(*), p(3′ UTR 50) = 0.013 (*), p(3′ UTR 100) = 0.0068 (**), p(3′ UTR 250) = 0.0009 (***), and p(3′ UTR 500) = 0.0071 (**). **e** RT-qPCR measurement of sfGFP transcripts in ZSWIM8 KO and Scr cells containing the sfGFP reporters. sfGFP transcript levels are normalized to *GAPDH* mRNA and the value in Scr cells expressing CDS trigger is set to 1. **f** Northern blot analyses of miR-16 in sfGFP reporter-expressing cells with ZSWIM8 KO. miR-7 is used as the positive control for ZSWIM8 KO, and miR-92a is used as a loading control. miRNA abundance is normalized to miR-92a. The miRNA abundance in Scr cells containing the sfGFP CDS reporters is set to 1. **g** The quantification of northern blots in (**f**). miR-16 levels are normalized to miR-92a and the value in Scr cells without Dox treatment is set to 1. p(lane 7/lane1)=0.0009 (***), p(lane 10/lane4)=0.0007 (***), p(lane8/lane7) =0.0384(*), p(lane9/lane7)=0.0099(**), p(lane11/lane10)=0.0036 (**), and p(lane12/lane10)=0.0042(**). **h** RT-qPCR measurement of the levels of AGO-associated sfGFP transcripts. RNA was extracted from AGO-IP in cells expressing the CDS or 3′ UTR trigger, with or without Dox induction. Statistically significant changes compared with the GFP control are indicated, $p = 0.0079$ (**). **i** RT-qPCR measurement of the levels of sfGFP transcripts. RNA was extracted from cells expressing the CDS or 3′ UTR trigger, with or without Dox induction. $p = 0.0061$(**). sfGFP transcript levels are normalized to *GAPDH* and the value in uninduced cells expressing the CDS trigger is set to 1. (Fig. 2e, h, i). All data are presented as mean ± SD ($n = 3$ biological replicates). Unpaired two-tailed t test calculated the p values, ns, not significant, $*p < 0.05$, $**p < 0.01$, $***p < 0.001$. Source data are provided as a Source Data file.

we also observed that repressing translation was less effective at increasing miR-16 TDMD induced by the 3′ UTR trigger (Fig. 3d and 3e, compare lane 9 to lanes 7, 8). Meanwhile, we used the NEDDylation inhibitor MLN4924, which has been shown to effectively inhibit the ZSWIM8-dependent ubiquitination on AGO[23], to confirm that inhibition of ZSWIM8 ubiquitination rescues miR-16 degradation induced by the CDS trigger (Fig. 3d and 3e, compare lane 6 to lane 3). Together, these data suggest that effectively clearing translational machinery away from the trigger site may improve the accessibility of the trigger to the miRNA, thereby enhancing the efficacy of ZSWIM8-dependent TDMD.

Ribosome stalling inducers enhance TDMD by CDS triggers

Having confirmed that inhibiting translation initiation of our reporter can improve miR-16 TDMD induced by a CDS trigger, we next explored whether globally blocking translating ribosomes is able to increase

https://doi.org/10.1038/s41467-025-60374-4

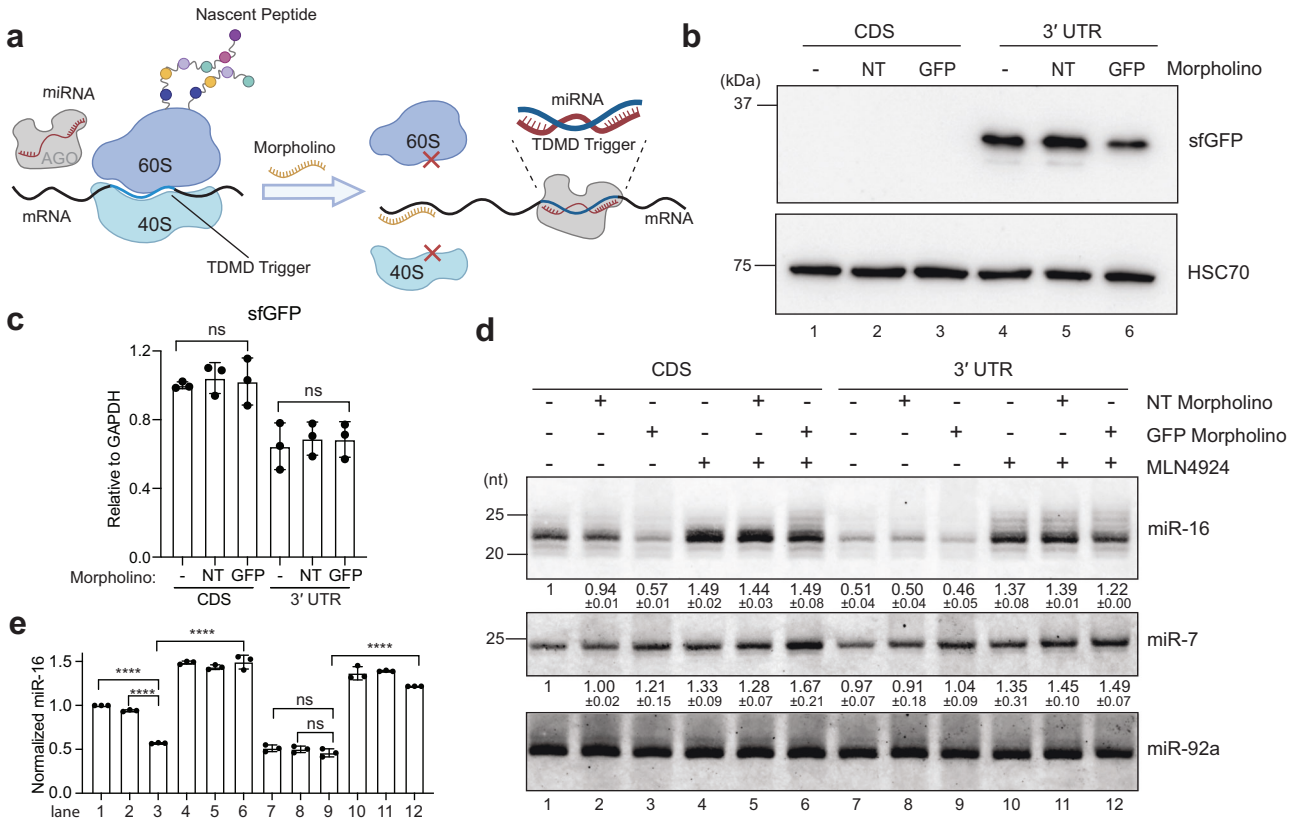

Fig. 3 | Blocking translation of sfGFP by morpholino oligo enhances TDMD mediated by the CDS trigger. a Schematic of morpholino oligonucleotide blocking translation initiation on the sfGFP mRNA transcript. **b** Western blot analysis of sfGFP protein level in trigger-expressing HEK293T cells with morpholino oligos treatment. HSC70 is used as a loading control. NT: Non-targeting. **c** RT-qPCR analyses of sfGFP mRNA levels in cells as in **b**. sfGFP mRNA levels are normalized to *GAPDH* and the value in cells expressing CDS trigger without morpholino oligos treatment is set to 1. Data are presented as mean ± SD ($n = 3$ biological replicates). Unpaired two-sided t-tests, ns, not significant. **d** The influence of morpholino oligos and neddylation inhibitor MLN4924 on miR-16. Representative northern blot analyses of miR-16, miR-7 and miR-92a in cells stably expressing sfGFP reporters with the CDS or 3′ UTR trigger. miR-7 serves as a positive control for MLN4924 treatment, which inhibits the ZSWIM8-mediated ubiquitination. miR-92a serves as a loading control. Relative miR-16 levels are shown as mean ± SD ($n = 3$ biological replicates). **e** The quantification of northern blots in **d**. Error bars represent SD, unpaired two-tailed t test calculated the p-values, ns, not significant, $*p < 0.05$, $**p < 0.01$, $***p < 0.001$, $****p < 0.0001$. p(lane 1/lane3)<0.0001 (****), *p*(lane2/lane3)<0.0001 (****), *p*(lane3/lane6)<0.0001 (****) and p(lane12/lane9)<0.0001 (****). Source data are provided as a Source Data file.

TDMD efficacy as well. To do this, we employed six translation inhibitors and surveyed their effects on miR-16 TDMD (Fig. 4a)[41–45]. Three of them, lactimidomycin (LTM), harringtonine (HTN), and cycloheximide (CHX), inhibit translation globally by blocking ribosome translocation. LTM is a compound that selectively inhibits the initiation of translation without interfering with ribosomes that have already bypassed the start codon[41]. The stably expressed CDS trigger induces miR-16 degradation more effectively in cells treated with LTM than untreated cells (Fig. 4b, compare lane 2 to lane 1; Fig. 4c left, compare red line to black line). In parallel, LTM treatment had no effect on miR-16 abundance in cells without Dox induction (Supplementary Fig. 3a). Thus, these findings indicate that the increased miR-16 degradation was caused by LTM reducing ribosome translocation on trigger transcripts. We also noticed an increased extent of tailing and trimming upon LTM treatment, which was accentuated under ZSWIM8 knockout (Fig. 4b and 4c, compare lanes 4 and 6 to lanes 3 and 5). In contrast, LTM treatment does not influence miR-16 degradation for the 3′ UTR trigger, and merely induces further tailing and trimming (Fig. 4b and 4d, right panels). Like LTM, HTN selectively targets translation initiation without affecting elongation[42]. On the other hand, CHX can block the initiation and elongation phase of translation[41]. Indeed, by using these three chemicals to globally limit ribosomal occupancy of mRNAs, we were able to "switch on" a normally ineffective CDS TDMD trigger to be as effective as the 3′ UTR trigger (Fig. 4b–4d, and Supplementary Fig. 3b and 3c).

Three other translation inhibitors, thapsigargin (Tg), tunicamycin (Tm), and histidinol (His-OH), can induce endoplasmic reticulum (ER) stress, phosphorylation of translation initiation factor eIF2α thereby globally inhibiting translation (Fig. 4a)[43–46]. However, we found that these treatments did not influence TDMD induced by the miR-16 CDS trigger (Fig. 4e–4g, and Supplementary Fig. 3d, 3e and 3f). We found these results puzzling and therefore sought to confirm that ER stress and ribosome stalling inducers could inhibit protein translation as expected. To do this, we utilized the puromycin staining assay that labels nascent peptides as a readout of global translation[47]. We found all six chemicals can inhibit global translation, whereas the ribosome stalling inducers (LTM, CHX, and HTN) were more effective at reducing translation than the stress inducers (Tg, Tm, and His-OH) (Fig. 4h, puromycin panel). However, the sfGFP translated from our reporter is minimally affected by ER stress inducers, while completely inhibited by the ribosome stalling inducers (Fig. 4h, sfGFP panel). It is known that certain transcripts containing inhibitory upstream open reading frame (uORF) can be selectively translated under global translation inhibition conditions induced by ER stress[48]. Although not by design, the sfGFP reporter may evade translation inhibition by a similar mechanism. Alternatively, overexpression of sfGFP transcripts may be

https://doi.org/10.1038/s41467-025-60374-4

translated in a cap-independent fashion or saturate the translation machinery so that it becomes resistant to eIF2α phosphorylation. In any case, our data show that the sfGFP reporter can evade the ER stress response and therefore ribosomes could still interfere with the CDS trigger under these conditions. Taken together, ribosome stalling enhances CDS trigger efficacy in inducing miR-16 decay in HEK293T cells.

Next, we further expanded our exploration to other known TDMD-regulated miRNAs, miR-7 and miR-221[11,17]. As discussed earlier, we have placed *CYRANO* trigger targeting miR-7 with the CDS region downstream of sfGFP (Supplementary Fig. 1). Notably, LTM treatment can also enhance the TDMD efficacy of *CYRANO* miR-7 trigger within CDS (Supplementary Fig. 3G, compare lane 3 to lane 2). Additionally, our group previously reported that *BCL2L11* contains a TDMD trigger

Fig. 4 | Translation inhibition facilitates TDMD when triggers locate in the coding region. a Illustration of the molecular mechanisms of six translation inhibitors. Northern blot analyses of miR-16 in ZSWIM8 KO and Scr cells containing the sfGFP CDS or 3′ UTR triggers treated with LTM (**b**) or TG (**e**) for 8 hours. miR-7 serves as a positive control for ZSWIM8 KO and miR-92a is used as a loading control. Relative miR-16 levels are shown as mean ± SD ($n = 3$ biological replicates). The influence of triggers by LTM (**d**) or TG (**g**) treatment on miR-16 length. Plotted are intensity values as a function of gel migration measured by line densitometry of northern blot in (**b**) or (**e**). Peaks correspond to lengths of miR-16 isoforms, as indicated (arrowheads). **c** and **f** The quantification of northern blots in **b** and **e**, respectively. Unpaired two-tailed t test calculated the p values, ns, not significant, $*p < 0.05$, $**p < 0.01$, $***p < 0.001$. In **c**, p(lane2/lane1) = 0.0053 (**), p(lane4/lane2) = 0.0179(*), p(lane6/lane2) = 0.0123(*), p(lane10/lane8) = 0.0075(**), p(lane12/lane8) = 0.0052(**). In (**f**) p(lane10/lane8) = 0.0003(***), p(lane12/lane8) = 0.0004(***). **h** Representative immunoblots detecting puromycin-labeled nascent proteins and sfGFP in HEK293T cells expressing the 3′ UTR trigger, treated with six translation inhibitors. Ponceau staining of the blot is used to quantify the total protein in each sample. Source data are provided as a Source Data file.

in the 3′ UTR that induces miR-221 degradation[11]. To test whether relocating the trigger sequence of this TDMD trigger to the CDS affects miRNA degradation, we removed the stop codon of the *BCL2L11* transcript to include the trigger sequence in CDS. We generated the HEK293T cell stably expressing the inducible *BCL2L11*-CDS construct. Northern blot analyses showed that *BCL2L11*-CDS can induce miR-221 degradation more effectively in cells treated with LTM than in untreated cells (Supplementary Fig. 3h, compare lane 3 to lane 2), accompanied by obvious tailing and trimming. Additionally, the miR-221 degradation induced by *BCL2L11*-CDS was rescued by ZSWIM8 KO (Supplementary Fig. 3h, compare lanes 6 and 9 to lane 3). Therefore, different CDS triggers, situated in the native sequence of *CYRANO* or *BCL2L11*, can be exposed by LTM-induced translation inhibition to induce miRNA degradation. These findings imply that the enhancement of the CDS trigger-induced miRNA degradation by blocking ribosomes is a broadly applicable phenomenon.

Ribosome stalling in HD cells increases CDS trigger TDMD efficacy

Global translation reductions may be linked to the pathogenesis of some neurodegenerative disorders. Such reductions could stem from alterations in the translational machinery or from inappropriate activation of the integrated stress response[49]. This suggests a potential interplay between translation dynamics and RNA-mediated regulatory processes, including TDMD, in disease contexts. For example, HD is a genetic neurodegenerative disease caused by an abnormally expanded CAG tri-nucleotide repeat in the *HTT* gene, which is thought to associate with ribosome stalling and repressed protein synthesis[35]. Meanwhile, altered miRNA expression in HD has been observed[50,51]. Whether and how global translational repression might regulate miRNA expression remains unclear.

Given our observations that global ribosome stalling increased CDS trigger efficacy on miR-16 in HEK293T cells, we then hypothesized that translation inhibition in HD cells will lead to miRNA dysregulation by TDMD through CDS triggers. Previously, a mouse striatal cell line was engineered to stably express *HTT* exon 1 with different numbers of CAG repeats that can be translated into a stretch of glutamine (Q)[52]. An increased stretch of Qs in HTT is both prognostic of HD and can be indicative of disease severity. Compared to control cells (ST$Hdh^{Q7/Q7}$, CTRL) and HD-heterozygous (ST$Hdh^{Q7/Q111}$, HD-hetro), HD-homozygous (ST$Hdh^{Q111/Q111}$, HD-homo) showed diminished puromycin incorporation, which reflects the global translational repression in this model (Fig. 5a). We therefore used this cell model to probe the impact of ribosome stalling on the efficacy of our CDS trigger against miR-16. We generated HD cell lines stably expressing our CDS trigger as well as ZSWIM8 KO. ZSWIM8 KO was validated by TIDE analyses (Fig. 5b), and northern blot analyses showed the rescue of miR-7 degradation under ZSWIM8 KO (Fig. 5c). Importantly, there was neither alteration to global translation repression following ZSWIM8 KO (Fig. 5d, compare lanes 4 and 6 to lane 2), nor influence on the abundance of sfGFP transcripts (Supplementary Fig. 4a). We next examined the TDMD efficacy of CDS trigger against miR-16 in these cells. Northern blot analyses showed that the CDS trigger can more effectively induce miR-16 degradation in mouse HD-homo cells than in CTRL cells (Fig. 5e, f, compare lane 8 to lane 2). Meanwhile, miR-16 can be stabilized to a similar level with ZSWIM8 KO in CTRL and HD-homo cells (Fig. 5e and 5f, compare lanes 10 and 12 to lanes 4 and 6). Therefore, reduced translation in HD can modulate TDMD mediated by a CDS trigger.

Identification of miRNAs sensitive to translation inhibition

To globally identify miRNAs that are degraded by endogenous CDS triggers in HEK293T cells, which express the sfGFP reporter targeting miR-16, we employed AQ-seq for accurate quantification of miRNAs[33]. Specifically, we screened the miRNAs that were significantly downregulated under LTM treatment but not significantly altered if ZSWIM8 is also knocked out (see "Materials and Methods"). We referred to these miRNAs as "translation-sensitive miRNAs" as they may be regulated by CDS triggers whose effectiveness depends on translation. Surprisingly, miR-16 is the only translation-sensitive miRNA identified with this selection criteria (Fig. 6a, b, and Supplementary Data 2, "1_LTM to DMSO" tab). The fact that miR-16's passenger strand is not translation-sensitive suggests that miR-16 is under TDMD-mediated destabilization. We next attempted to screen for translation-sensitive miRNAs with an orthogonal analysis method. Essentially, we select for miRNAs that are more sensitive to ZSWIM8 loss under translational inhibition. First, we identified ZSWIM8-sensitive miRNAs in control (DMSO) (Fig. 6c) and translational inhibition (LTM) groups (Fig. 6d). Known ZSWIM8-sensitive miRNAs, miR-7 and miR-503 were upregulated upon ZSWIM8 KO (Fig. 6c and 6d), supporting the validity of our experimental approach. Subsequently, the miRNAs with more pronounced increase following ZSWIM8 KO in LTM treatment compared with control treatment were grouped as translation-sensitive miRNAs (Supplementary Data 2) (see "Methods"). Similarly, there seem to be limited translation-sensitive miRNAs in HEK293T cells as only miR-16, miR-195 and miR-1247 were identified (Fig. 6d).

To further explore the translation-sensitive miRNAs in mouse striatal cells where translation inhibition is induced by mutant *Htt*, we performed AQ-seq on CTRL and HD-homo cells. For technical reasons, these cells do not contain the sfGFP reporter for miR-16 TDMD (see "Materials and Methods"). Using two translation-sensitive miRNA identification methods applied in HEK293T cells, we first identified miR-449c, miR-3535, miR-25 and miR-20a that are more degraded in mouse striatal scramble cells than in ZSWIM8 KO cells (Fig. 6e, 6f). On the other hand, comparison of ZSWIM8-sensitivity in control and HD-homo cells presented miR-485, miR-154, miR-543, miR-495, miR-450b, miR-503 and miR-7a as translation-sensitive miRNAs (Fig. 6g, h). Many translation-sensitive miRNAs were previously classified as ZSWIM8-sensitive[24,26,27]. Nonetheless, these miRNAs could potentially be subject to additional CDS-triggers under translation inhibition. As controls, we confirmed that known ZSWIM8-sensitive miRNAs, miR-7a, miR-503, miR-335, miR-337 and miR-341, were upregulated in ZSWIM8 knockout cells (Supplementary Data 3). Even though we applied very generous selection criteria, the translation-sensitive miRNAs identified by two orthogonal approaches do not overlap. We conclude that, apart from miR-16 as a positive example in HEK293T cells, a very short list of miRNAs may be targeted for degradation by endogenous CDS triggers (Supplementary Data 2 and 3).

https://doi.org/10.1038/s41467-025-60374-4

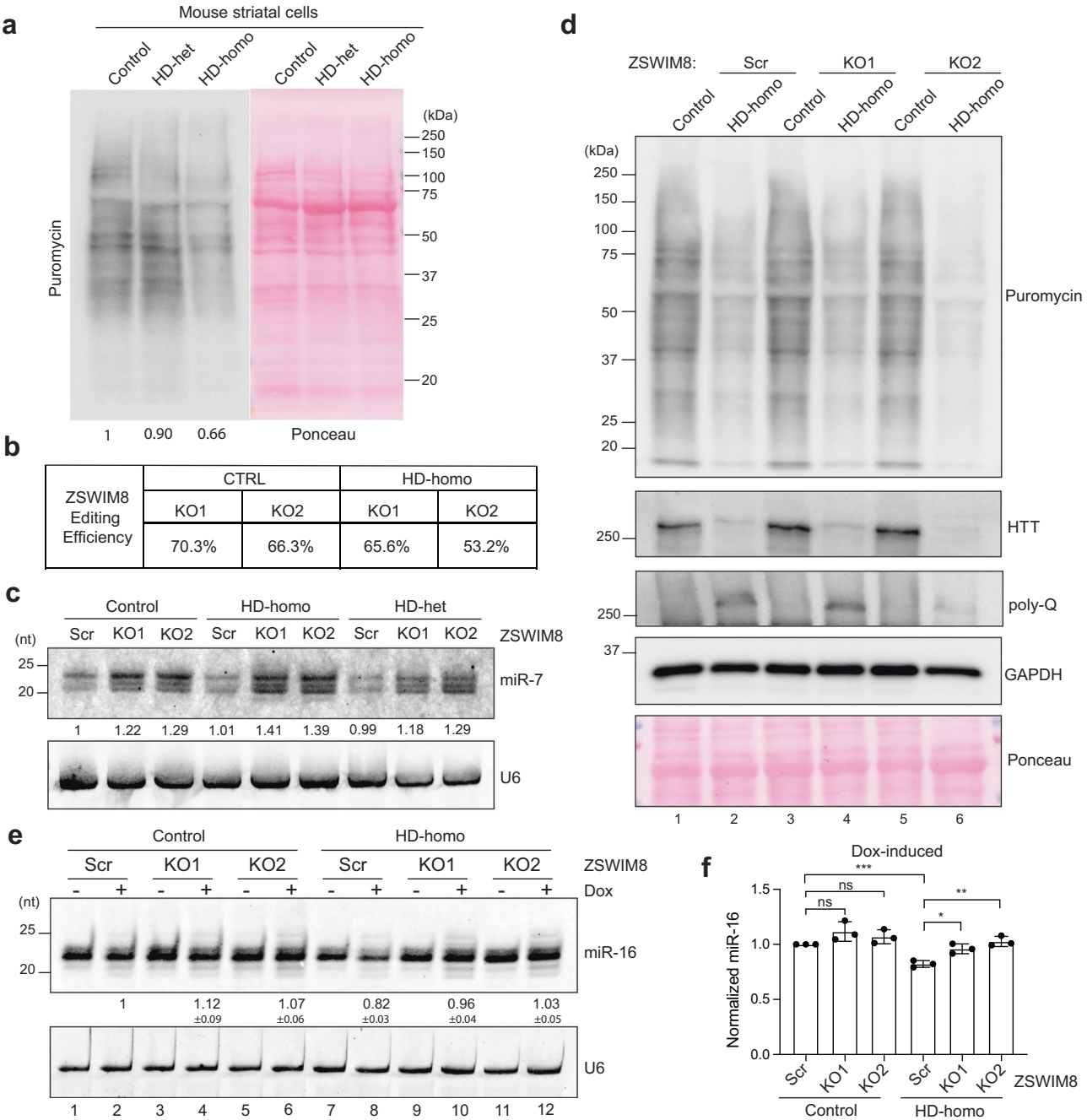

Fig. 5 | TDMD is affected in cell models of Huntington's Disease. **a** Representative immunoblots of metabolic labeling of nascent proteins, using puromycin, in Control, HD-het and HD-homo mouse striatal cells ($n = 3$ biological replicates). Ponceau staining of the blot was used to quantify the total protein in each lane. The value in Control cells is set to 1. **b** TIDE analyses showing indel efficiency at the targeted site in mouse striatal cells with ZSWIM8 knockout mediated by CRISPR-Cas9. **c** Northern blot analyses of miR-7 in Control, HD-het and HD-homo mouse striatal cells with or without ZSWIM8 KO. U6 is used as a loading control. Relative miR-16 levels are shown as mean ± SD ($n = 3$ biological replicates). **d** Representative western blot of puromycin-labeled nascent protein, HTT, Poly-Q and GAPDH in Control and HD-homo mouse striatal cells with ZSWIM8 KO. Ponceau staining and GAPDH are used as loading controls ($n = 3$ biological replicates). **e** Northern blot analyses of miR-16 in mouse striatal Control or HD-homo cells expressing Dox-inducible sfGFP reporter containing the CDS trigger against miR-16. ZSWIM8 knockout status was indicated on top of the blots. U6 is used as a loading control. Relative miR-16 levels are shown as mean ± SD ($n = 3$ biological replicates). **f** The quantification of northern blots in (**e**). Error bars represent SD, unpaired two-tailed t test calculated the p values, ns, not significant, $*p < 0.05$, $**p < 0.01$, $***p < 0.001$. p (HD-homo Scr/Control Scr)=0.0005 (***), p(HD-homo KO1/Scr)=0.0114(*), and p(HD-homo KO2/Scr)=0.003(**). Source data are provided as a Source Data file.

Screening for potential CDS triggers

We next looked for CDS triggers corresponding to translation-sensitive miRNAs in LTM-treated HEK293T cells and HD-homo mouse striatal cells. To do this, we performed AGO-CLASH that can capture inter-molecularly ligated miRNA-target RNA hybrids[32,53,54]. In HEK293T cells, as a benchmark of CDS trigger-miRNA hybrids, an increase of sfGFP: miR-16 hybrids was observed upon LTM treatment in scramble cells, with a greater increase noted in LTM-treated ZSWIM8 KO cells (Supplementary Fig. S5a). AGO-CLASH detected only one translation-sensitive miRNA (miR-20a) forming hybrids with potential TDMD triggers localizing in the CDS region (Supplementary Data 4, yellow highlights in "293T potential TDMD hyb"; hybrid count > 10

https://doi.org/10.1038/s41467-025-60374-4

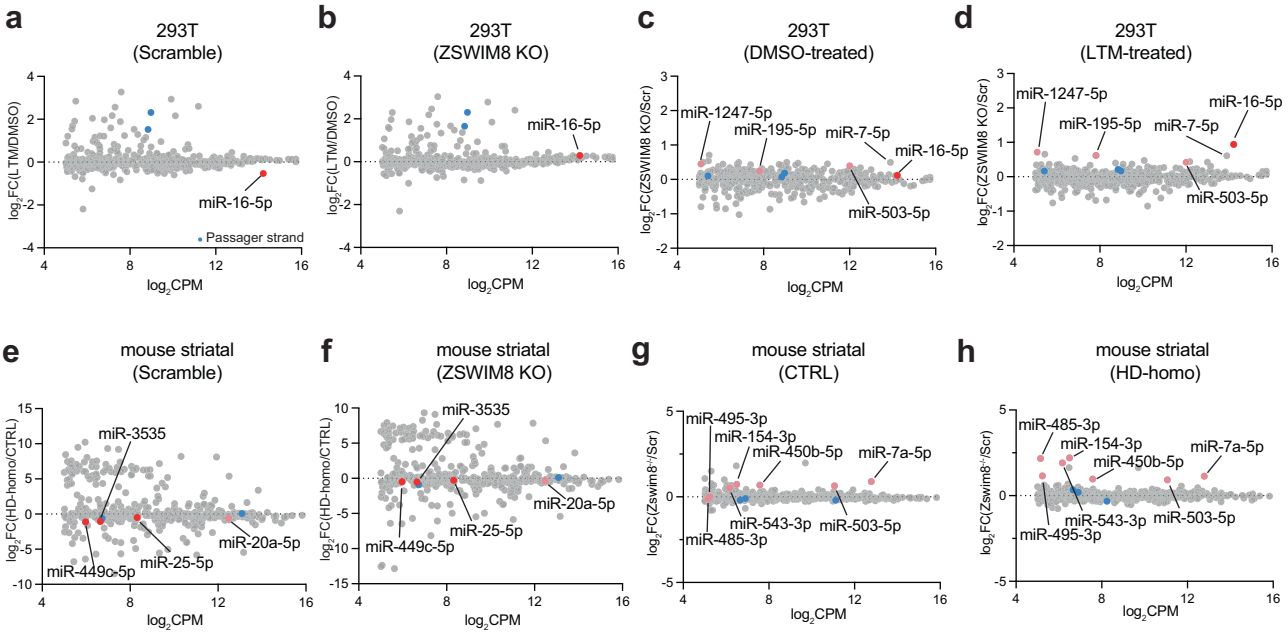

Fig. 6 | Screening for "translation-sensitive" miRNAs. The influence of LTM treatment on miRNA abundance in HEK293T cells expressing the sfGFP reporter containing the miR-16 CDS trigger in scramble cells (**a**) and in ZSWIM8 KO cells (**b**). The influence of ZSWIM8 knockout on miRNA abundance in cells with vehicle control (DMSO) treatment (**c**) or LTM treatment (**d**). Average value from 3 AQ-seq experiments were plotted. miRNA fold changes are plotted, comparing miRNA levels in HD-homo to CTRL mouse striatal cells with scramble (**e**) or ZSWIM8 KO (**f**). The influence of ZSWIM8 knockout on miRNA abundance in mouse striatal CTRL cells (**g**) or HD-homo cells (**h**). Average value from 2 AQ-seq experiments were plotted. Translation-sensitive miRNAs are highlighted in red and pink (the pink dots denote previously annotated ZSWIM8-sensitive miRNAs), while their passenger strands are highlighted in blue. Source data are provided as a Source Data file.

RPM and increase 2-fold in LTM treatment, detailed in "Materials and Methods"): *VTA1* (vesicle trafficking 1): miR-20a. Besides miR-20a, *VTA1* also forms hybrids with other miR-17 family members, including miR-17 and miR-93. The only other candidate hybrid harboring a CDS trigger is *ITGA8* (integrin subunit alpha 8): miR-222, though miR-222 was not classified as a translation-sensitive miRNA. Overall, these two candidates of miRNA-CDS trigger hybrids have the highest read counts following sfGFP: miR-16 in AGO-CLASH. These hybrids showed more than 2-fold increase in abundance in LTM-treated HEK293T cells, which is consistent with sfGFP: miR-16 (Supplementary Fig. 5b, c, and Data 4). Also, the base-pairing profile of these putative CDS triggers (Supplementary Fig. 5d) agrees well with the previously reported TDMD base-pairing pattern in the validated triggers (Fig. 1).

We next examined whether these putative TDMD triggers can affect the abundance of their corresponding miRNAs. Therefore, we designed three CRISPR-Cas9 sgRNAs targeting the surrounding region of potential *ITGA8* and *VTA1* triggers. Pairs of two plasmids targeting each trigger were co-transduced in HEK293T cells by lentivirus. For each trigger KO, three pairs of sgRNAs were used to obtain three different stable polyclonal cells. From these stable cells, we performed PCR analyses on the trigger region of genomic DNA and Sanger sequencing to check the triggers' integrity (Supplementary Fig. 5e–h). Three pairs of sgRNAs either knocked out or mutated the trigger region of *ITGA8* (Supplementary Fig. 5e, g) and *VTA1* (Supplementary Fig. 5f and 5h). However, upon trigger deletion, there was no change observed for miRNAs potentially targeted by these putative triggers, with or without LTM treatment (Supplementary Fig. 5I, miR-222, compare lanes 3-8 to lanes 1-2 and 9-10; miR-20a, compare lanes 11-16 to lanes 1-2 and 9-10). Meanwhile, we observed that a decrease in miR-222 upon LTM treatment regardless of the putative *ITGA8* trigger, which indicates that translational repression influences miR-222 through another trigger or an unrelated mechanism (Supplementary Fig. 5I, compare LTM+ lanes to LTM- lanes).

Because AGO-CLASH hybrids with high abundance did not reveal bona fide CDS triggers, we next specially searched for AGO-CLASH hybrids that can form base pairs mimicking the most effective TDMD interaction, *CYRANO*: miR-7. Accordingly, we identified that the *TNFSF12* (tumor necrosis factor superfamily, member 12) transcript can form hybrids with the miR-17 family members (miR-20a, miR-17, miR-93, and miR-106) (Fig. 7a). Note that miR-20a, a known ZSWIM8-sensitive miR-17 family member[26], is also identified as a translation-sensitive miRNA in mouse striatal cells (Fig. 6e). There were very few counts of *TNFSF12*: miR-17 family hybrids in our AGO-CLASH datasets (Supplementary Data 4). Nonetheless, the base-pairing pattern formed by *TNFSF12* and miR-17 family members closely mimics that of *CYRANO*: miR-7 and an artificial trigger previously designed by Kleaveland et al. to effectively degrade miR-17 in HEK293T cells by transient transfection (Fig. 7b)[17]. The miR-17 trigger within *TNFSF12* only differs from the artificial miR-17 trigger by 2 nucleotides, with the predicted base-pairing being identical. We transiently transfected the sfGFP CDS and 3′ UTR reporter plasmids with the *TNFSF12* trigger sequence in HEK293T cells. Northern blot analyses show that the *TNFSF12* trigger within both the CDS and 3′ UTR can induce miR-17 and miR-20a degradation (Fig. 7c, compare lanes 1 and 2 to lane 4). Consistent with the above-mentioned finding that translation inhibits TDMD, the CDS trigger is less effective than the 3′ UTR trigger (Fig. 7c, compare lane 1 to lane 2). Notably, overexpression of the *TNFSF12* transcript independent of the sfGFP reporter also induces miR-17 and miR-20a degradation (Fig. 7c, compare lane 3 to lane 4). LTM treatment does not significantly increase miR-17 degradation for the CDS trigger, probably due to over-saturation of the trigger transcripts by transient transfection (Fig. 7c, compare lane 5 to lane 1).

To evaluate the miR-17 family degradation induced by *TNFSF12* at a more physiological level, we generated a cell model stably expressing doxycycline-inducible full-length *TNFSF12* transcript. Additionally, we made five *TNFSF12* mutants with different binding patterns to the miR-17 family and a deletion mutant (Fig. 7d). RNA sequencing experiments revealed that Dox-induced *TNFSF12* expression did not affect other genes (Supplementary Fig. 6a), and the abundance of *TNFSF12* remained unchanged regardless of the LTM treatment (Supplementary

https://doi.org/10.1038/s41467-025-60374-4

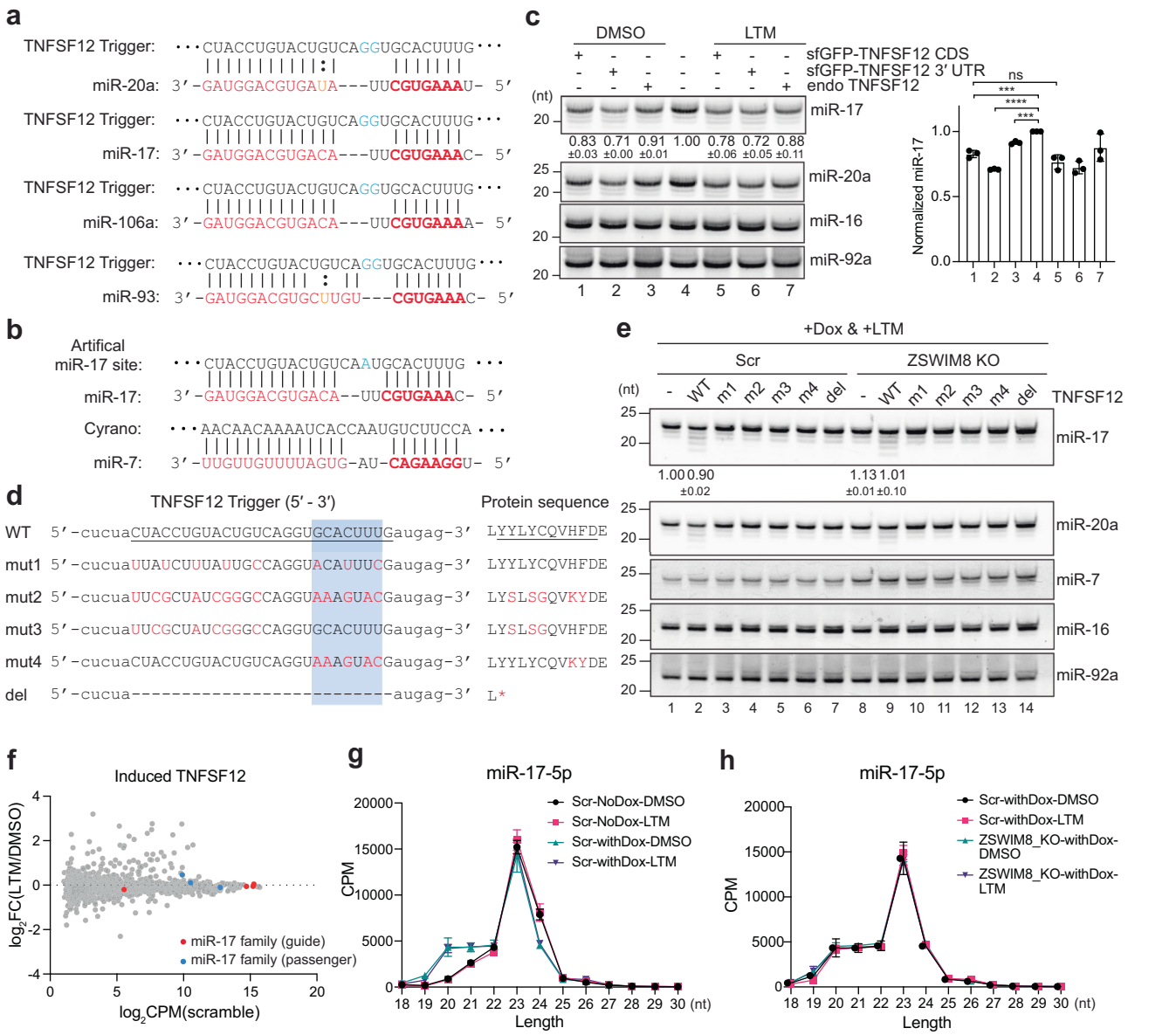

Fig. 7 | Screening for endogenous CDS triggers. a Base-pairing pattern of miR-17 family members with the putative TDMD trigger located in the CDS region of *TNFSF12*. **b** Base-pairing pattern of miR-7 with the *CYRANO* trigger. The same base pairing pattern is maintained in an engineered trigger targeting miR-17[17]. Nucleotides differ in the engineered trigger and *TNFSF12* trigger are highlighted in cyan. **c** Representative northern blot measuring miR-17 and miR-20a levels in HEK293T cells transiently transfected with sfGFP reporter plasmids containing the putative *TNFSF12* trigger within the CDS or 3′UTR region, or a plasmid encoding the wildtype full-length *TNFSF12* transcript either with or without LTM treatment. miR-92a and miR-16 are used as loading controls. Relative miRNA abundance is indicated below the blots. The level of miR-17 in HEK293T parental cells is set to 1. Data are presented as mean ± SD ($n = 3$ biological replicates). The quantification of the northern blot is shown on the right. Unpaired two-tailed t test calculated the p values, ns, not significant, $*p < 0.05$, $**p < 0.01$, $***p < 0.001$, $****p < 0.0001$. p(lane1/lane4)=0.0005 (***), p(lane2/lane4)<0.0001 (****), and p(lane3/lane4)=0.0002 (***). **d** Schematic of the WT *TNFSF12* trigger constructs with mutated miR-17 sites. Mutations are highlighted in red. The encoded amino acid sequences are shown on the right. **e** Northern blot analyses of miR-17 and miR-20a in ZSWIM8 KO and Scr cells containing the induced *TNFSF12* triggers treated with LTM for 8 hours. miR-7 served as a positive control of ZSWIM8 KO, and miR-16 and miR-92a are used as loading controls. Relative miR-17 levels are shown as mean ± SD ($n = 3$ biological replicates). **f** The miRNA levels fold change upon LTM treatment in Dox-induced scramble cells expressing the *TNFSF12* WT. **g** The fraction of AQ-seq reads of miR-17 (18–30 nt) in the HEK293T cells containing Dox-inducible *TNFSF12* trigger. Combination of Dox and LTM treatments is indicated. **h** Fraction graph of AQ-seq reads as in (**g**), except that the combination of LTM treatment and ZSWIM8 knockout is indicated. Data are presented as mean ± SD ($n = 3$ biological replicates). Source data are provided as a Source Data file.

Fig. 6b). More importantly, *TNFSF12* levels were within the range of other native transcripts (Supplementary Fig. 6a and 6b). With Dox induction and addition of LTM, miR-17 was marginally degraded (~10%) by *TNFSF12* WT, accompanied by miRNA trimming, as shown by northern blot (Fig. 7e, compare lane 2 to lane 1). miR-17 degradation was not observed in the absence of *TNFSF12* induction (Dox) or translation inhibition (LTM) (Supplementary Fig. 6c, d). As controls, we did not observe changes in miR-17 abundance or isoform pattern in *TNFSF12* mutants that disrupted basepairing with miR-17 (Fig. 7e, and Supplementary Fig. 6c and 6d, compare lanes 3-7 to lane 2). We further performed AQ-seq on cell stably expressing the inducible *TNFSF12* WT transcript to accurately measure alterations to the abundance of miR-17 family members. However, according to EdgeR analysis, the miR-17 family members did not significantly decrease in LTM-treated cells (Fig. 7f, and Supplementary Data 5)[55]. Interestingly, we observed trimming of all miR-17 family members (miR-17, miR-20a, miR-106a

and miR-93) induced by *TNFSF12* WT transcript (Fig. 7e, g, and Supplementary Fig. 6d–g, Data 5), which occurred independently of ZSWIM8 (Fig. 7h and Supplementary Fig. 6h–j, Data 5). Therefore, when driven by an inducible promoter, *TNFSF12* triggers can specifically induce trimming and may marginally induce degradation of all miR-17 family members.

To further test how the endogenous *TNFSF12* trigger may regulate the miR-17 family, we screened for cells with high *TNFSF12* mRNA expression. A search in a publicly available database (Human Protein Atlas, proteinatlas.org) revealed high *TNFSF12* expression in lung cancer cells[56]. We performed RT-qPCR experiments to measure *TNFSF12* mRNA levels in ten immortalized human cell lines including A375 and A549 lung cancer cells. A549 and MDA-MB-231 cells have the highest *TNFSF12* mRNA expression (Supplementary Fig. 7a and 7b). To expose the potential CDS trigger within *TNFSF12* mRNA, we used morpholino oligos targeting the translation start site of *TNFSF12* in A549 and MDA-MB-231 cell lines. Western blot analyses showed TNFSF12 protein was repressed by morpholino treatment (Supplementary Fig. 7c and 7d). However, miR-17 level did not decrease when TNFSF12 translation was repressed in A549 (Supplementary Fig. 7e, compare lane 2 to lane 1) or MDA-MB-231 (Supplementary Fig. 7f, compare lane 3 to lanes 1 and 2). LTM or CHX induced global translation inhibition also did not induce miR-17 degradation either in A549 (Supplementary Fig. 7h, compare lanes 3 and 5 to lane 1) or in MDA-MB-231 (Supplementary Fig. 7i, compare lane 3 to lane 1). Finally, we used CRISPR-Cas9 with two sgRNAs to knockout the potential TDMD trigger region in the endogenous *TNFSF12* transcript and confirmed by Sanger sequencing (Supplementary Fig. 7g). Consistent with previous experiments, miR-17 level was not affected by trigger knockout when translation was inhibited in A549 (Supplementary Fig. 7h, compare lane 4 to lane 3 and lane 6 to lane 5) and MDA-MB-231 cells (Supplementary Fig. 7i, compare lane 4 to lane 2). Taken together, although *TNFSF12* exhibits extensive base-pairing with miR-17 family members, it is unlikely to contain an endogenous CDS trigger that can lead to miRNA degradation in the cell lines we examined.

Discussion

In contrast to most target sites for endogenous miRNA identified within RISC-mediated RNA silencing pathway or TDMD pathway, which are predominantly located in the 3′ UTR region of target mRNAs, siRNAs can target nearly any region of an mRNA and remain fully functional[57,58]. This raises the question of why siRNAs can target the coding region of mRNAs, whereas miRNAs typically cannot. Previous research suggests that this difference may be due to siRNAs usually having full complementarity with the coding regions of their target mRNAs, while miRNAs exhibit only partial complementarity[1]. Specifically, canonical miRNA-induced silencing complex (miRISC) activities involve base-pairing primarily within the "seed" region (nucleotides 2-8, or a 7mer). Despite miRNAs' extensive base-pairing (an additional 7-14 nucleotides) at the 3′ end in TDMD, increasing RNA duplex stability, such TDMD-triggered sites are still all located in non-coding regions[13,36]. Our work aims to bridge the knowledge gap by elucidating miRNA's preference for extensive base-pairing with RNA triggers in non-coding regions, rather than CDS regions, during TDMD. Furthermore, we intend to answer the question: what's the criterion for identifying endogenous TDMD trigger?

TDMD base-pairing pattern

The binding pattern of RNA duplex between TDMD trigger and miRNA may partially answer the above question. The binding pattern of validated metazoan TDMD duplexes involves a seed match, the presence of extensive base pairing at the 3′ end, and an internal bulge[37] (Fig. 1). However, these requirements could be quite loose. For example, the degradation of miR-35 family is Ebax-1 (worm ortholog of ZSWIM8)-dependent in *C. elegans*, but the sequence of miR-35 family 3′ end is dispensable, whereas the requirement for the seed is maintained. Notably, extensive base pairing at the 3′ end is not only to induce miRNA degradation (TDMD) but usually accompanied by tailing or trimming of the miRNA, termed "target directed tailing and trimming" (TDTT)[20,37,59]. We noticed that our sfGFP CDS trigger not only induced miR-16 degradation but also substantially induced TDTT, which can be detected by northern blot analyses (Fig. 2c), and further confirmed by AQ-seq (Supplementary Fig. 8a). These isoforms mainly result from 3′ end tailing. TDTT of miR-7 by the *CYRANO* trigger is primarily resulting from the terminal nucleotidyltransferase, TENT2[17]. As reported previously, TENT2-mediated TDTT was not required for *CYRANO*-induced miR-7 decay, as blocking miRNA 3′ end nucleotide with 2′-O-methyl group did not block TDMD[17,24]. In line with this, we observed that TENT2 is similarly dispensable on our artificial miR-16 trigger (Supplementary Fig. S8b, compare lanes 4 and 6 to lane 2, lanes 10 and 12 to lane 8). Northern blot analyses revealed that LTM treatment, coupled with TENT2 knockout, prevents miR-16 tailing and promotes the accumulation of its predominant isoform (Supplementary Fig. 8b, compare lanes 4 and 6 to lane 2). Similarly, inducible *TNFSF12* can trigger miR-17 family trimming, but not degradation (Fig. 7g and Supplementary Fig. 6e–g). This further supports that TDTT and TDMD are independent processes, although both are triggered by extensive pairing of miRNA to the target. While TDTT depends on the accessibility of miRNA 3′ end to TENTs, TDMD depends on conformational change of AGO to recruit ZSWIM8. Our understanding of how the same base-pairing pattern between miRNA and the trigger facilitates miRNA degradation or tailing/ trimming is still emerging.

Another outstanding question is what determines an AGO-miRNA complex to undergo miRNA-mediated target repression or TDMD? It appears that target repression or miRNA degradation are mutually exclusive. Deletion of a TDMD trigger does not influence the trigger mRNA's abundance, suggesting that trigger mRNA is not under miRNA-mediated repression[11,18]. As discussed above, a distinct AGO conformation induced by TDMD base-pairing is believed to recruit ZSWIM8[23,24,37]. Unlike TDMD base-pairing that involves extensive 3′ base-pairing (≥7 basepairs), miRNA-mediated repression often involves only "3′ supplementary pairing" to miRNA nucleotides 13-16. As such, deadenylase and decapping enzymes are recruited to facilitate target RNA degradation. Therefore, structural conformation of AGO and associated proteins is a core feature in determining whether AGO-miRNA complex undergoes miRNA degradation or target RNA degradation. However, recent studies in *C. elegans* indicate that certain TDMD events may not involve extensive 3′ base-pairing, demonstrating the complexity of this miRNA regulatory pathway[25].

Accessibility of a TDMD trigger can be influenced by translation

To fully elucidate the criteria for TDMD trigger identification, beyond the structural basis of miRNA base-pairing modalities with TDMD triggers, a systematic understanding of the localization preferences of TDMD triggers is essential. Our study provides evidence that TDMD trigger localization and spaciotemporal control is associated with TDMD efficacy. It appears that the accessibility of miRNA-AGO complex to triggers is a key determinant of trigger efficacy, where ribosomes and translational machinery normally reduce AGO association with triggers within the CDS (Fig. 2f and 2g).

Our study reveals that a CDS reporter trigger becomes more effective when the cells are treated with ribosome stalling inducers, as seen in HEK293T cells (Figs. 2–4), and with repressed protein synthesis in a mouse HD cell model (Fig. 5). We demonstrated that CDS triggers against different miRNAs and within different sequence contexts could similarly induce miRNA degradation when translation is inhibited (Figs. 4b, 5e, 7e, and Supplementary Fig. 3a, 3b, 3g and 3h). It points to a broader possibility of CDS triggers inducing TDMD in other disorders associated with ribosome stalling. Diamond-Blackfan Anemia (DBA) is

a congenital syndrome associated with anemia, physical malformations and cancer[60,61]. In the majority of individuals with DBA, mutations or gene deletions are detected in a subset of ribosomal proteins[62]. The pool of available ribosomes is limited, while ribosome composition remains constant. Interestingly, this global reduction in ribosome levels more profoundly alters translation of a select subset of transcripts[62]. Therefore, if there are TDMD triggers localized within the CDS region of these transcripts, ribosome stalling may facilitate the accessibility of these CDS triggers to certain miRNAs.

Additionally, inappropriate stalling of ribosomes during protein synthesis is closely linked to the presence of proteotoxic components and cellular stress and is associated with the pathogenesis of neurodegenerative diseases. In a mouse model of neurodegeneration, the combined loss of function of a neuron-specific arginine tRNA and GTPBP2, a GTPase involved in ribosome recycling, resulted in an increase in ribosome stalling and activation of the kinase GCN2[63]. Furthermore, collided ribosomes have also been implicated in the activation of GCN2, which leads to the phosphorylation of eIF2α, a key regulator of cap-dependent translation, as part of the integrated stress response[64]. Although our CDS trigger reporter failed to respond to ER stress, one type of the integrated stress response (Fig. 4e–4h), GCN2 responds to another type of stress induced by amino acid starvation. However, the underlying mechanisms, including the sensing of deacylated tRNAs and ribosome stalling, are not fully understood[46]. Therefore, it is worth to examine whether the activation of GCN2 influences the regulation of TDMD by CDS triggers.

In addition to the experiments involving ER stress stated above (Fig. 4), we also tested our miR-16 CDS trigger in several other cellular conditions with reduced translation, including mitosis, hypoxia and oxidative stress. Many studies have reported that global translation is repressed during mitosis[65–67]. RO-3306, a selective CDK1 inhibitor, induces G2 arrest of the cell cycle and effectively synchronizes cells into the M phase[68]. However, since M phase typically lasts for less than 1 hour, the time may be limited for TDMD induced by CDS triggers[68]. This potentially explains the lack of miR-16 TDMD upon RO-3306 treatment (Supplementary Fig. 9a). Hypoxia, oxygen deficiency in cells, often represses basal protein synthesis in tumor cell lines by preventing cap-dependent translation initiation but activates hypoxia-responsive mRNA[69–71]. Cobalt (II) Chloride hexahydrate ($CoCl_2$) is a chemical inducer of hypoxia-inducible factor[72]. Our northern blot showed that $CoCl_2$ treatment on CDS trigger-expressing cells did not increase miR-16 degradation levels (Supplementary Fig. 9b). Thus, sfGFP reporter translation may not be influenced by hypoxia. Hydrogen peroxide (H_2O_2)-induced oxidative stress globally influences translation[73,74]. Low concentrations of H_2O_2 result in increased protein synthesis; in contrast, a high dose of H_2O_2 may inhibit protein synthesis. Therefore, we applied a gradient dose of H_2O_2 to reduce protein synthesis[73,74]. However, the CDS trigger in the sfGFP reporter does not induce TDMD in response to oxidative stress (Supplementary Fig. 9c). Taken together, the pathway of TDMD is complex, and our miR-16 CDS trigger reporter did not respond to all global translational repression inducers.

Unless the translational machinery is fully cleared out of the mRNA transcripts, it could be difficult for CDS triggers to access miRNA for long enough time to fully induce TDMD. However, we did identify several miRNAs whose level decreased upon translation inhibition. We also identified a potential trigger for the miR-17 family localized to the CDS region of *TNFSF12* transcript, which was sufficient to induce degradation when overexpressed in HEK293T cells. *TNFSF12* transcripts are merely expressed in HEK293T cells, which could explain why we did not observe the increased *TNFSF12*: miR-17 hybrids under LTM treatment in AGO-CLASH. However, in cell lines tested, we could not confirm that endogenously expressed *TNFSF12* can degrade the miR-17 family. Taken together, our study indicates that naturally occurring CDS triggers are rare even under ribosome stalling conditions. However, there may be more subtle examples of CDS triggers yet to be explored in the AGO-CLASH hybrids (Supplementary Data 4). Although the endogenous CDS triggers are rare, our discovery of translation repression as a contributing factor to the efficacy of TDMD provides a more comprehensive understanding of the extent that should be considered for a potential TDMD trigger. Future research is needed to explore other factors that could influence the trigger accessibility to benefit TDMD events, such as RNA modifications and potential RNA structures surrounding the TDMD trigger.

Methods

Cell Lines

HEK293T cells were cultured in Dulbecco's modified Eagle's medium (DMEM, Sigma #D5796) supplemented with 10% fetal bovine serum (FBS, Life Tech #A5256701), 1% penicillin-streptomycin (ThermoFisher #15140163) at 37 °C with 5% CO_2. Mouse striatal cells (ST*Hdh*) expressing knock-in wild-type human *HTT* exon1 with 7 glutamine (Q) repeats (control; STHdh^{Q7}/Q^{7}, #CH00097) or 111 glutamine repeats (HD-het; ST$HdhQ^{7}/Q^{111}$ #CH00096, and HD-homo; ST$HdhQ^{111}/Q^{111}$ #CH00095) were purchased from the Coriell Institute for Medical Research and cultured in DMEM medium supplemented with 10% FBS, 1X GlutaMax (Gibco #35050061), 1% penicillin/streptomycin at 33 °C with 5% CO_2. For cells stably expressing doxycycline-inducible reporters, Tet-tested FBS (R&D Systems Inc #S10350) was used. All cell lines were routinely passaged when reaching ~80% confluency.

As advised by the Coriell Institute for Medical Research, mouse striatal HD cells are recommended to be kept below passage number 14 (P14) to maintain a representative of HD. Given that we received these cells at P8, we had difficulty constructing ZSWIM8 KOs together with miR-16 CDS trigger reporter and preformed AGO-CLASH within the passage limit. At P16 and P18, miR-16 degradation induced by CDS trigger is ablated (compare Supplementary Fig. 4b and 4c to Fig. 5e), likely due to loss of translational repression beyond P14 (Supplementary Fig. 4d). Therefore, to identify potential HD-associated CDS triggers, we had to perform CLASH and AQ-seq in CTRL and HD-homo cells (P12) without the CDS trigger reporter.

Plasmid Construction

For TDMD trigger expression via plasmid transfection, we cloned artificial miR-16, miR-7, or miR-17 TDMD triggers, with or without ~200 nt flanking regions (*CYRANO* for miR-16/miR-7 and *TNFSF12* for miR-17), into the CDS or 3′ UTR of sfGFP in the AVA2590 plasmid (Addgene #85442) using MluI restriction sites. Additionally, the full-length *TNFSF12* transcript independent of the sfGFP reporter was cloned into the same plasmid via the same restriction site.

For generation of cell lines stably expressing doxycycline-inducible TDMD triggers, the artificial miR-16 or miR-7 TDMD trigger sequence (within CDS or 3′ UTR of sfGFP) from the plasmids used for transfection were PCR-amplified and inserted into pENTR_D TOPO (ThermoFisher # K240020) via NotI and AscI sites. For *BCL2L11* or *TNFSF12* TDMD trigger cell lines, *BCL2L11* sequences (with ΔBH3 mutations, incapable of inducing apoptosis) or full-length *TNFSF12* transcript were PCR-amplified from HEK293T cDNA and inserted into pENTR_D TOPO (Thermo Fisher) via NotI and AscI sites. Subsequently, the inserts in pENTR plasmids were inserted into pB-TA-ERP2 (Addgene #80479) with the LR clonase II (ThermoFisher #11791020) to generate pB-TA-ERP2-sfGFP-miR-16, pB-TA-ERP2-sfGFP-miR-7, pB-TA-ERP2-*BCL2L11*-miR-221 and pB-TA-ERP2-*TNFSF12*-miR-17.

Inducible Cell Line Generation

Polyclonal HEK293T and mouse striatal HD cell lines stably expressing a doxycycline-inducible TDMD trigger were generated by co-transfection of the pB-TA-ERP2-sfGFP-miR-16, pB-TA-ERP2-sfGFP-miR-7, pB-TA-ERP2-*BCL2L11*-miR-221 or pB-TA-ERP2-*TNFSF12*-miR-17 and transposase plasmids (gift from Eric Wang lab) by Lipofectamine 3000

(ThermoFisher #L3000015) according to the manufacturer's protocol. Puromycin selection began 24 h following transfection, at a concentration of 1 μg/ml. Cells without GFP expression were enriched by FACS under no Dox induction to minimize leaky expression of the construct.

CRISPR-Cas9 Mediated Gene Knockout

Lentiviruses for knockout were generated by transfecting cells with lentiCRISPR_v2_vectors [Addgene #98291 (hygromycin-resistant); #52961(puromycin-resistant); #98293(blasticidin-resistant)] containing sgRNAs against the target genes. 80% confluent HEK293T cells in 10 cm dishes were transfected with virus packaging plasmids (6 μg of psPAX2 and 4 μg pMD2.G) and 10 μg LentiCRISPR_v2 plasmids encoding a control sgRNA, a sgRNA against ZSWIM8, a sgRNA against TENT2, or a sgRNA flanking endogenous triggers with Lipofectamine 3000. After transfection, the cells were cultured in FreeStyle 293 Expression Medium (Gibco #12338018) for 48 h, and the supernatant containing the viruses was harvested. 1 mL lentivirus with 4 μg/ml polybrene was used to infect HEK293T and mouse striatal cells in 6-well plates for 48 h. The cells were selected in the media with selection agents for up to a week [1 μg/mL puromycin, 150 μg/ml hygromycin (Fisher #10687010), or 5 μg/ml blasticidin (InvivoGen #ant-bl-1)]. Polyclonal knockout efficiency was determined by PCR amplification of genomic DNA at the targeted locus, followed by TIDE analysis[75]. KO efficiency (%) was provided from the TIDE analysis website with default settings (https://tide.nki.nl/) by uploading the sgRNA sequence, Sanger sequencing files (.ab1 format) of control and KO samples. Genotyping primers for TIDE analysis and sgRNA sequences are listed in Supplementary Data 1.

Sucrose density gradient

Following 24-hrs Dox induction, HEK293T cells were treated with the cycloheximide (Sigma Aldrich, 01810) at 100 μg/ml for 5 min. Cells were harvested and added with lysis buffer [20 mM Tris pH 7.5, 150 mM NaCl, 15 mM $MgCl_2$, 1 mM DTT, 100 μg/ml cycloheximide, 1× Halt™ Protease and Phosphatase Inhibitor Cocktail (EDTA-free) (Thermo Fisher, 78443), 100 U/ml SUPERase In (Ambion, AM2696), 20 U/ml TURBO DNase (Ambion, AM2239), 1% TritonX-100, and 8% glycerol. To fractionate ribosomes, cell lysate was layered onto 15-45 % (w/v) of sucrose gradient (sucrose, 20 mM Tris, pH 7.5, 150 mM NaCl, 5 mM $MgCl_2$, 1 mM DTT, 100 μg/ml cycloheximide) and centrifuged by 13,500 xg for 2.5 hrs at 4 °C using the SW60Ti rotor.

RNA Isolation and RT-qPCR

The cells adhered to the tissue culture plates were washed with phosphate buffer-saline (PBS), and RNA was isolated using TRIzol (ThermoFisher #15596018) following the manufacturer's protocol. The cDNA synthesis was performed using a reverse transcription kit (QIAGEN #205313). All RT-qPCR experiments used GAPDH mRNA for normalization. The qPCR primers used are listed in Supplementary Data 1.

Immunoprecipitation of AGO-Associated RNAs

10 million cells were washed with cold PBS and scraped, followed by centrifuging at 500 xg for 5 min at 4°C. Cell pellets were resuspended in 600 μL NP-40 lysis buffer (1% NP-40, 10% glycerol, 150 mM NaCl, 50 mM Tris-HCl, 5 mM EDTA) and lysed with gentle rotation at 4°C for 30 min. After centrifugation at 16000 xg, at 4°C for 15 min, the supernatant was collected (10% saved as input) and incubated with 1x protease inhibitor cocktail (Sigma #5056489001), Superase•In RNase inhibitor (ThermoFisher #AM2696), 5 μg AGO 4F9 antibody/IgG and 40 μL protein L beads (ThermoFisher #88850) then rotated at 4°C overnight. The beads were washed by Buffer D buffer (1% NP-40, 20 mM pH7.9 HEPES, 0.1 M KCl, 0.2 mM EDTA, 10% glycerol with fresh added 0.5 mM PMSF) twice and the bound RNAs were extracted by TRIzol reagent. The amount of target transcripts in both the input and AGO-IP samples was analyzed with RT-qPCR.

Western Blot

Total protein was extracted with NP-40 lysis buffer and quantified using DC protein assay kit (Bio-Rad #5000113). Equal amount of protein samples were analyzed in 10% polyacrylamide-SDS gel and then transferred to 0.45 μM nitrocellulose membranes (BIO-RAD #1620115). The membranes were blocked in 5% non-fat milk, and then incubated in primary and secondary antibodies. The following commercial antibodies were used at the indicated dilution: anti-GFP (Santa Cruz #sc-9996, 1:5000), anti-Huntingtin (Sigma #MAB2166, 1:3000), anti-puromycin (Sigma #MABE343, 1:1000), anti-polyglutamine (Sigma #P1874, 1:500), anti-GAPDH (Sigma #G9645, 1:10000), goat anti-Rabbit IgG (Life Tech #31460, 1:5000) and goat anti-mouse IgG (Life Tech #31430, 1:5000).

Puromycin Metabolic Labeling and Immunoblotting

Cells were plated at a confluency of about 60–70%. The day after seeding, 20 μM puromycin (ThermoFisher #A1113803) was added to the medium for 5 min. After removal of the medium, the cells were rinsed twice with cold 1x PBS and immediately lysed in 1% NP-40 buffer containing protease inhibitors. Protein lysates were used for western blotting experiments. The puromycin incorporation was normalized to the ponceau S staining.

Northern Blot

Northern blotting analysis of RNA was performed similar to near-infrared (IR) northern blot as previously described[76]. Briefly, total RNA was isolated by TRIzol according to the manufacturer's protocol and separated on 18% denaturing urea polyacrylamide gel. Then total RNA was transferred to a Whatman Nytran N membrane (VWR #28151-360) and EDC (N-(3-dimethylaminopropyl)-N′-ethylcarbodiimide) (ThermoFisher #22981) cross-linked. The probes used in this study are listed in Supplementary Data 1. The images were acquired by Typhoon IR scanner and analyzed with ImageQuant TL (v7.0).

Translation inhibitor and proteosome inhibitor treatment

MLN4924 (Sigma #5054770001), MG-132 (Sigma #474790), Lactimidomycin (Sigma # 5062910001), Harringtonine (LKT Laboratories #H0169), Cyclohexamide (Sigma #01810), Thapsigargin (Sigma #T9033), Tunicamycin (Sigma #T7765), Histidinol (Sigma H8125), $CoCl_2$ (Sigma #C8661), and RO3306 (Sigma #SML0569) were dissolved in dimethyl sulfoxide (DMSO, Life Tech #85190). Cells were treated with DMSO alone, or one of the following inhibitors (2.5 μM LTM, 100 μg/ml CHX, 2 μM HTN, 200 nM TG, 5 μg/ml Tm, 2.5 mM His-OH, 100 μM $CoCl_2$, 10 μM RO-3306 for 8 hours. For inducible cell lines, cells were pre-treated with Dox induction for 16 hours to express trigger transcripts. Cells were treated with DMSO alone or 2 μM MLN4924 for 24 hours with Dox induction, or 10 μM MG-132 for 0-8 hours with Dox induction.

Vivo-morpholino oligonucleotides were dissolved in nuclease-free water. 1×10^6 cells/well were seeded in 6-well plates and incubated with 5 μM vivo-morpholino oligos against sfGFP or *TNFSF12* translation initiation site, or a control oligo. After 24-hour treatment, the total RNA was extracted for the northern blot. Morpholino oligo sequences are listed in Supplementary Data 1.

AQ-seq

Libraries were prepared as previously described[33]. In brief, 20 μg of total RNA with 1 μl of 10 nM synthetic miRNA spike-in RNA oligos (Supplementary Data 1) was isolated and size-selected between 17-30 nt on a 15% polyacrylamide urea gel. Purified RNA was ligated to a pre-adenylated 3′ adaptor (/5rApp/NNNNTGGAATTCTCGGGTGCCAAGG/3ddC/) using T4 RNA ligase 2 KQ (NEB #M0373L) in a reaction supplemented with 20% PEG8000 (NEB). After gel purification on a 15% polyacrylamide urea gel, RNA was ligated to a 5′ adaptor (5′-rGrUrUrCrArGrArGrUrUrCrUrArCrA rGrUrCrCrGrArCrGrArUrCrNrNrNrN-

3′) using T4 RNA ligase 1 (NEB #M0437M) in a reaction supplemented with 20% PEG8000. RNA was reverse transcribed with SuperScript III (Life Tech #18080044), and the cDNA was amplified 8-12 cycles with NEBNext high-fidelity DNA polymerase (NEB #M0541L). Amplified DNA was purified on a 6% PAGE gel. Libraries were sequenced on the Illumina NovaSeq X Plus by Admera Health.

AGO-CLASH

AGO-CLASH was performed as previously described[12,34] with modifications according to chimeric-eCLIP[53]. Briefly, AGO-IP was carried out with Pierce Protein L magnetic beads (Thermo Fisher #88850) conjugated with monoclonal anti-AGO antibody (clone 4F9, UF ICBR) and incubated with cell lysate overnight at 4°C (40 μg of antibody and 40 μl of magnetic beads for 3 mg total lysate). The RNA bound with AGO was phosphorylated by T4 PNK (3′ phosphatase minus) enzyme (NEB #M0236S) on the beads. The inter-molecular ligation of the miRNA with target RNA was performed on-bead at 4°C overnight with T4 RNA ligase I (NEB #M0437M). Then, on-bead samples were dephosphorylated with FastAP (Thermo Fisher #EF0651) and then followed by T4 PNK treatment (NEB #M0236L), and a pre-adenylated adapter (5′-/5rApp/NNNNTGGAATTCTCGGGTGCCAAGG/3ddC/-3′) was ligated to the 3′ end of the RNA fragments by T4 RNA Ligase 2, truncated K227Q (NEB #M0351L). Following NuPAGE gel electrophoresis, samples were transferred to 0.45 μm nitrocellulose membrane (Cytiva #10600002), and eluted from the membrane. RNA was reverse transcribed by Superscript IV reverse transcriptase (ThermoFisher #18090050) with primer (5′-GCCTTGGCACCCGAGAATTCCA-3′). ExoSAP-IT (ThermoFisher #78201) was applied to remove excess oligonucleotides. 5′ linker oligo (5′-/5Phos/NNNNGATCGTCGGACTGTAGAACTCTGAAC/3SpC3/-3′) ligates to the 5′ end of cDNA at room temperature for overnight. The cDNA libraries were generated as previously described[34]. Libraries were separated and size selected between 147 and 527 bp. AGO-CLASH libraries were sequenced on the Illumina NovaSeq X Plus by Admera Health.

Data analyses

The adapter sequences of raw reads were trimmed using Cutadapt software[77] (version 2.10), and reads shorter than 18 nucleotides were discarded. Paired FASTQ files were assembled using Pear software[78] (version 0.9.11) with default settings. Subsequently, the assembled reads were collapsed using fastx_collapser from the FASTX Toolkit[79] to remove PCR duplications. The collapsing process was based on the identification of four random nucleotides at both the 5′ and 3′ ends of the reads. The clean reads underwent additional trimming to remove the random nucleotides using Cutadapt software (version 2.10).

For AQ-seq: clean reads were initially aligned to a miRNA database from miRbase, including spike-in sequences, utilizing the custom 'CLASH.py' script (in https://github.com/UF-Xie-Lab). This mapping process was executed with the following command: python3 CLASH.py all_miRNA_isoform_table_2nd_18th -i [--input] <clean.fasta > -d [--miRNA_database]. The alignment criteria were designed to capture the diversity of miRNA isoforms and total miRNA counts, incorporating four specific requirements: (1) an allowance for a two-nucleotide extension at the 5′ end of miRNAs, ensuring the inclusion of slightly elongated isoforms; (2) a strict alignment condition where the sequence from the 1st to the 18th nucleotide of the miRNA must perfectly match the reads, thereby prioritizing the core sequence integrity of miRNAs; (3) a provision for miRNAs to possess a 3′ tail extending up to a maximum length of 30 nucleotides, accommodating variations in miRNA length; and (4) recognition of miRNA tails as being either templated or non-templated, allowing for a comprehensive analysis of miRNA processing variations. The CLASH.py script also generated read counts for each miRNA and spike-in. Samples were normalized using total reads and differential expression analysis of miRNA abundance was completed using the Bioconductor package EdgeR[55] (version 3.42.4) in the generalized linear model (GLM) mode.

To screen for the translation-sensitive miRNAs, only the miRNAs that are above the abundance threshold are considered ($\log_2$CPM > 5). The criteria were that the miRNA significantly decreased ($\log_2 FC\left(\frac{LTM}{DMSO}\right) < -0.3$, FDR < 0.01) in scramble cells under translation inhibition conditions (LTM or HD-homo), and the abundance of miRNAs was not significantly influenced by translation inhibition in ZSWIM8 KO cells (FDR > 0.05). The orthogonal analysis method for the translation-sensitive miRNAs primarily considers their sensitivity to ZSWIM8 KO. With ZSWIM8 KO, the miRNAs need to increase ($\log_2 FC\left(\frac{ZSWIM8KO}{Scrabmle}\right) > 0.3$, FDR < 0.01) in translation-inhibited cells. Meanwhile, this ZSWIM8-sensitivity is lower in control cells, e.g. ($\log_2 FC\left(\frac{ZSWIM8KO}{Scrabmle}\right) in\ LTM - \log_2 FC\left(\frac{ZSWIM8KO}{Scramble}\right) in\ DMSO > 0.2$). Note that ZSWIM8-sensitive miRNAs in the control cells can still be classified as translation-sensitive miRNAs.

For CLASH: Processed reads underwent mapping to the reference genome, hybrid calling, base-pairing prediction, and annotation by the Hyb software with default settings[80]. Note that in the default settings, the target RNA reads were extended 25 nt on the 3′ end to compensate for possible deletion of the sequences that can base-pair with the miRNA. Custom Python scripts were developed to screen and identify candidate TDMD hybrids based on specific criteria according to reported TDMD pairs and involved four key factors: (1) base pairing of the miRNA seed region (nucleotides 2-8) with the target RNA, allowing G-U wobble pairs; (2) presence of more than seven consecutive base pairs between the 3′ end of the miRNA and the target RNA within the last 8 nucleotides, or nine consecutive base pairs not necessarily involving the last 8 nucleotides; (3) a central bulge of the target RNA/miRNA hybrids of less than 7 nucleotides but greater than 0 nucleotides; and (4) a predicted binding energy between the miRNA and the target RNA lower than 16 kcal/mol.

To identify potential TDMD triggers within the CDS region, two additional criteria were applied. Firstly, the RNA target: miRNA hybrid reads in AGO-CLASH from DMSO-treated cells or HD control cells are required to be higher than 10 reads per million (RPM). Secondly, a more than 2-fold increase in miRNA/target RNA hybrid reads in AGO-CLASH from LTM-treated compared to DMSO-treated cells or in HD-homo mouse striatal cells compared to control cells. These hybrids were highlighted in yellow in Supplementary Data 4, tab "293T potential TDMD hyb".

Reporting summary

Further information on research design is available in the Nature Portfolio Reporting Summary linked to this article.

Data availability

The data supporting the findings of this study are available from the corresponding authors upon request. All sequencing data that support the findings of this study have been deposited in the National Center for Biotechnology Information Sequence Read Archive (SRA) through the BioProject PRJNA1093144. Source data for the figures and Supplementary Figs. are provided as a Source Data file. Source data are provided with this paper.

Code availability

All custom scripts have been made available at https://github.com/UF-Xie-Lab/Translational-regulation-of-TDMD and in the Zenodo repository https://doi.org/10.5281/zenodo.15278039.

References

1. Bartel, D. P. *Metazoan MicroRNAs*. *Cell* **173**, 20–51 (2018).
2. Bail, S. et al. Differential regulation of microRNA stability. *RNA* **16**, 1032–1039 (2010).

3. Krol, J. et al. Characterizing light-regulated retinal microRNAs reveals rapid turnover as a common property of neuronal microRNAs. *Cell* **141**, 618–631 (2010).
4. Gantier, M. P. et al. Analysis of microRNA turnover in mammalian cells following Dicer1 ablation. *Nucleic Acids Res* **39**, 5692 (2011).
5. Guo, Y. et al. Characterization of the mammalian miRNA turnover landscape. *Nucleic Acids Res* **43**, 2326–2341 (2015).
6. Duffy, E. E. et al. Tracking distinct RNA populations using efficient and reversible covalent chemistry. *Mol. Cell* **59**, 858–866 (2015).
7. Marzi, M. J. et al. Degradation dynamics of microRNAs revealed by a novel pulse-chase approach. *Genome Res* **26**, 554–565 (2016).
8. Kingston, E. R. & Bartel, D. P. Global analyses of the dynamics of mammalian microRNA metabolism. *Genome Res* **29**, 1777–1790 (2019).
9. Reichholf, B. et al. Time-resolved small RNA sequencing unravels the molecular principles of MicroRNA homeostasis. *Mol. Cell* **75**, 756–768 (2019).
10. Schirle, N. T., Sheu-Gruttadauria, J. & MacRae, I. J. Structural basis for microRNA targeting. *Science* **346**, 608–613 (2014).
11. Li, L. et al. Widespread microRNA degradation elements in target mRNAs can assist the encoded proteins. *Genes Dev.* **35**, 1595–1609 (2021).
12. Sheng, P. et al. Screening of Drosophila microRNA-degradation sequences reveals Argonaute1 mRNA's role in regulating miR-999. *Nat. Commun.* **14**, 1–14 (2023).
13. Hiers, N. M., Li, T., Traugot, C. M. & Xie, M. Target-directed microRNA degradation: mechanisms, significance, and functional implications. *Wiley Interdiscip. Rev. RNA* **15**, e1832 (2024).
14. Bitetti, A. et al. MicroRNA degradation by a conserved target RNA regulates animal behavior. *Nat. Struct. Mol. Biol.* **25**, 244–251 (2018).
15. Marcinowski, L. et al. Degradation of cellular mir-27 by a novel, highly abundant viral transcript is important for efficient virus replication in vivo. *PLoS Pathog.* **8**, e1002510 (2012).
16. Ghini, F. et al. Endogenous transcripts control miRNA levels and activity in mammalian cells by target-directed miRNA degradation. *Nat. Commun.* **9**, 1–15 (2018).
17. Kleaveland, B., Shi, C. Y., Stefano, J. & Bartel, D. P. A network of noncoding regulatory RNAs Acts in the mammalian brain. *Cell* **174**, 350–362.e17 (2018).
18. Kingston, E. R., Blodgett, L. W. & Bartel, D. P. Endogenous transcripts direct microRNA degradation in Drosophila, and this targeted degradation is required for proper embryonic development. *Mol. Cell* **82**, 3872–3884.e9 (2022).
19. Cazalla, D., Yario, T. & Steitz, J. Down-regulation of a host MicroRNA by a herpesvirus saimiri noncoding RNA. *Science (1979)* **328**, 1563–1566 (2010).
20. Ameres, S. L. et al. Target RNA-directed trimming and tailing of small silencing RNAs. *Science (1979)* **328**, 1534–1539 (2010).
21. Libri, V. et al. Murine cytomegalovirus encodes a miR-27 inhibitor disguised as a target. *Proc. Natl Acad. Sci. USA* **109**, 279–284 (2012).
22. Lee, S. et al. Selective degradation of host MicroRNAs by an intergenic HCMV noncoding RNA accelerates virus production. *Cell Host Microbe* **13**, 678–690 (2013).
23. Han, J. et al. A ubiquitin ligase mediates target-directed microRNA decay independently of tailing and trimming. *Science (1979)* **370**, eabc9546 (2020).
24. Shi, C. Y. et al. The ZSWIM8 ubiquitin ligase mediates target-directed microRNA degradation. *Science (1979)* **370**, eabc9359 (2020).
25. Donnelly, B. F. et al. The developmentally timed decay of an essential microRNA family is seed-sequence dependent. *Cell Rep.* **40**, 111154 (2022).
26. Shi, C. Y. et al. ZSWIM8 destabilizes many murine microRNAs and is required for proper embryonic growth and development. *Genome Res* **33**, 1482–1496 (2023).
27. Jones, B. T. et al. Target-directed microRNA degradation regulates developmental microRNA expression and embryonic growth in mammals. *Genes Dev.* **37**, 661–674 (2023).
28. Grimson, A. et al. MicroRNA targeting specificity in mammals: determinants beyond seed pairing. *Mol. Cell* **27**, 91–105 (2007).
29. Gu, S., Jin, L., Zhang, F., Sarnow, P. & Kay, M. A. Biological basis for restriction of microRNA targets to the 3′ untranslated region in mammalian mRNAs. *Nat. Struct. Mol. Biol.* **16**, 144–150 (2009).
30. Bartel, D. P. MicroRNAs: target recognition and regulatory functions. *Cell* **136**, 215–233 (2009).
31. Hsieh, A. C. et al. A library of siRNA duplexes targeting the phosphoinositide 3-kinase pathway: determinants of gene silencing for use in cell-based screens. *Nucleic Acids Res.* **32**, 893–901 (2004).
32. Helwak, A., Kudla, G., Dudnakova, T. & Tollervey, D. Mapping the human miRNA Interactome by CLASH reveals frequent noncanonical binding. *Cell* **153**, 654–665 (2013).
33. Kim, H. et al. Bias-minimized quantification of microRNA reveals widespread alternative processing and 3 end modification. *Nucleic Acids Res* **47**, 2630–2640 (2019).
34. Fields, C. J. et al. Sequencing of argonaute-bound microRNA/mRNA hybrids reveals regulation of the unfolded protein response by microRNA-320a. *PLoS Genet* **17**, e1009934 (2021).
35. Eshraghi, M. et al. Mutant Huntingtin stalls ribosomes and represses protein synthesis in a cellular model of Huntington disease. *Nat. Commun. 2021* **12**, 1–20 (2021).
36. Buhagiar, A. F. & Kleaveland, B. To kill a microRNA: emerging concepts in target-directed microRNA degradation. *Nucleic Acids Res* **52**, 1558–1574 (2024).
37. Sheu-Gruttadauria, J. et al. Structural basis for target-directed microRNA degradation. *Mol. Cell* **75**, 1243–1255.e7 (2019).
38. Yamamoto, S. et al. A drosophila genetic resource of mutants to study mechanisms underlying human genetic diseases. *Cell* **159**, 200–214 (2014).
39. Jones, A. N. et al. An evolutionarily-conserved RNA structure in the functional core of the lincRNA Cyrano. *RNA* **26**, 1234–1246 (2020).
40. Corey, D. R. & Abrams, J. M. Morpholino antisense oligonucleotides: Tools for investigating vertebrate development. *Genome Biol.* **2**, 1–3 (2001).
41. Lee, S. et al. Global mapping of translation initiation sites in mammalian cells at single-nucleotide resolution. *Proc. Natl Acad. Sci. USA* **109**, E2424–E2432 (2012).
42. Ingolia, N. T., Brar, G. A., Rouskin, S., McGeachy, A. M. & Weissman, J. S. The ribosome profiling strategy for monitoring translation in vivo by deep sequencing of ribosome-protected mRNA fragments. *Nat. Protoc.* **7**, 1534 (2012).
43. Walter, P. & Ron, D. The unfolded protein response: From stress pathway to homeostatic regulation. *Science (1979)* **334**, 1081–1086 (2011).
44. Kaufman, R. J. Stress signaling from the lumen of the endoplasmic reticulum: Coordination of gene transcriptional and translational controls. *Genes Dev.* **13**, 1211–1233 (1999).
45. Hansen, B. S., Vaughan, M. H. & Wang, L. Reversible inhibition by histidinol of protein synthesis in human cells at the activation of histidine. *J. Biol. Chem.* **247**, 3854–3857 (1972).
46. Harding, H. P. et al. The ribosomal P-stalk couples amino acid starvation to GCN2 activation in mammalian cells. *Elife* **8**, e50149 (2019).
47. Schmidt, E. K., Clavarino, G., Ceppi, M. & Pierre, P. SUnSET, a nonradioactive method to monitor protein synthesis. *Nat. Methods 2009* **6**, 275–277 (2009).
48. Palam, L. R., Baird, T. D. & Wek, R. C. Phosphorylation of eIF2 facilitates ribosomal bypass of an inhibitory upstream ORF to enhance CHOP translation. *J. Biol. Chem.* **286**, 10939–10949 (2011).
49. Kapur, M., Monaghan, C. E. & Ackerman, S. L. Regulation of mRNA Translation in Neurons–A Matter of Life and Death. *Neuron* **96**, 616 (2017).

50. Lee, S. T. et al. Altered microRNA regulation in Huntington's disease models. *Exp. Neurol.* **227**, 172–179 (2011).
51. Guo, S. et al. MicroRNA editing patterns in Huntington's disease. *Sci. Rep. 2022* **12**, 1–14 (2022).
52. Trettel, F. et al. Dominant phenotypes produced by the HD mutation in STHdhQ111 striatal cells. *Hum. Mol. Genet* **9**, 2799–2809 (2000).
53. Manakov, S. A. et al. Scalable and deep profiling of mRNA targets for individual microRNAs with chimeric eCLIP. *bioRxiv* **13**, 480296 (2022).
54. Gay, L. A., Turner, P. C. & Renne, R. Modified cross-linking, ligation, and sequencing of hybrids (qCLASH) to identify microRNA Targets. *Curr. Protoc.* **1**, e257 (2021).
55. Robinson, M. D., Mccarthy, D. J. & Smyth, G. K. edgeR: a Bioconductor package for differential expression analysis of digital gene expression data. *Bioinform. APPLICATIONS NOTE* **26**, 139–140 (2010).
56. Uhlen, M. et al. Towards a knowledge-based human protein atlas. *Nat. Biotechnol.* **28**, 1248–1250 (2010).
57. Martinez, J., Patkaniowska, A., Urlaub, H., Lührmann, R. & Tuschl, T. Single-stranded antisense siRNAs guide target RNA cleavage in RNAi. *Cell* **110**, 563–574 (2002).
58. Bartel, D. P. MicroRNAs: genomics, biogenesis, mechanism, and function. *Cell* **116**, 281–297 (2004).
59. Han, J. & Mendell, J. T. MicroRNA turnover: a tale of tailing, trimming, and targets. *Trends Biochem Sci.* **48**, 26–39 (2023).
60. Halperin, D. S. & Freedman, M. H. Diamond-blackfan anemia: etiology, pathophysiology, and treatment. *Am. J. Pediatr. Hematol. Oncol.* **11**, 380–394 (1989).
61. Vlachos, A., Rosenberg, P. S., Atsidaftos, E., Alter, B. P. & Lipton, J. M. Incidence of neoplasia in diamond blackfan anemia: a report from the diamond blackfan anemia registry. *Blood* **119**, 3815–3819 (2012).
62. Farrar, J. E. et al. Ribosomal protein gene deletions in diamond-blackfan anemia. *Blood* **118**, 6943 (2011).
63. Ishimura, R. et al. Ribosome stalling induced by mutation of a CNS-specific tRNA causes neurodegeneration. *Science* **345**, 455–459 (2014).
64. Yan, L. L. & Zaher, H. S. Ribosome quality control antagonizes the activation of the integrated stress response on colliding ribosomes. *Mol. Cell* **81**, 614–628.e4 (2021).
65. Tanenbaum, M. E., Stern-Ginossar, N., Weissman, J. S. & Vale, R. D. Regulation of mRNA translation during mitosis. *Elife* **4**, e07957 (2015).
66. Stonyte, V., Boye, E. & Grallert, B. Regulation of global translation during the cell cycle. *J. Cell Sci.* **131**, jcs220327 (2018).
67. Datta, B., Datta, R., Mukherjee, S. & Zhang, Z. Increased phosphorylation of eukaryotic initiation factor 2α at the G2/M boundary in human osteosarcoma cells correlates with deglycosylation of p67 and a decreased rate of protein synthesis. *Exp. Cell Res* **250**, 223–230 (1999).
68. Vassilev, L. T. et al. Cell cycle synchronization at the G2/M phase border by reversible inhibition of CDK1. **5**, 2555–2556 (2006).
69. Ho, J. J. D., Schatz, J. H., Uniacke, J. & Lee, S. Jekyll and hyde: activating the hypoxic translational machinery. *Trends Biochem Sci.* **46**, 171–174 (2021).
70. Ivanova, I. G., Park, C. V. & Kenneth, N. S. Translating the hypoxic response—the role of HIF protein translation in the cellular response to low oxygen. *Cells 2019* **8**, 114 (2019).
71. Genuth, N. R. & Barna, M. Heterogeneity and specialized functions of translation machinery: from genes to organisms. *Nat. Rev. Genet. 2018* **19**, 431–452 (2018).
72. Piret, J. P., Mottet, D., Raes, M. & Michiels, C. $CoCl_2$, a Chemical inducer of hypoxia-inducible factor-1, and hypoxia reduce apoptotic cell death in hepatoma cell line HepG2. *Ann. N. Y Acad. Sci.* **973**, 443–447 (2002).
73. Wozniak, M. A. & Chen, C. S. Mechanotransduction in development: a growing role for contractility. *Nat. Rev. Mol. Cell Biol.* **10**, 34–43 (2009).
74. Emara, M. M. et al. Hydrogen peroxide induces stress granule formation independent of eIF2α phosphorylation. *Biochem Biophys. Res Commun.* **423**, 763–769 (2012).
75. Brinkman, E. K., Chen, T., Amendola, M. & Van Steensel, B. Easy quantitative assessment of genome editing by sequence trace decomposition. *Nucleic Acids Res* **42**, e168–e168 (2014).
76. Miller, B. R., Wei, T., Fields, C. J., Sheng, P. & Xie, M. Near-infrared fluorescent northern blot. *RNA* **24**, 1871–1877 (2018).
77. Martin, M. Cutadapt removes adapter sequences from high-throughput sequencing reads. *EMBnet J.* **17**, 10–12 (2011).
78. Zhang, J., Kobert, K., Flouri, T. & Stamatakis, A. PEAR: a fast and accurate Illumina Paired-End reAd mergeR. *Bioinformatics* **30**, 614–620 (2014).
79. Gordon, A. & Hannon, G. J. Fastx-toolkit. FASTQ/A short-reads pre-processing tools. *Unpublished* http://hannonlab.cshl.edu/fastx_toolkit (2010).
80. Travis, A. J., Moody, J., Helwak, A., Tollervey, D. & Kudla, G. Hyb: a bioinformatics pipeline for the analysis of CLASH (crosslinking, ligation and sequencing of hybrids) data. *Methods* **65**, 263–273 (2014).

Acknowledgements

We thank Drs. Narry V. Kim, Lien Nguyen, Maurice Swanson, Srinivasa Subramaniam, Eric Van Nostrand and Eric Wang for reagents, protocols and suggestions. We thank members of the Xie lab for discussion, Dr. Vikas Dongardive for proofreading and the UF Interdisciplinary Center for Biotechnology Research for antibody production support. This work is supported by grants from the National Institutes of Health (R35GM128753 and R01CA282812 to M.X., T32AI007110 to C.M.T.), the American Cancer Society (Research Scholar Award RSG-21-118-01-RMC to M.X.), the Japan Science and Technology Agency (JPMJPR2049 to K.F.). J.B. is supported by NIH R01AG076234, R56AG069880, RF1AG084178, R01AG084236 and R01AG083039.

Author contributions

Conceptualization, M.X. and T.L.; most experiments were performed by T.L. with assistance from P.S., J.F.EM., N.M.H., Y.W., P.A., K.F. and Y.L.; bioinformatics, L.L., T.L. and C.M.T.; writing – original draft, T.L., N.M.H. and M.X.; writing – review & editing, T.L., L.L., N.M.H., C.M.T. and M.X.; supervision, M.X.; funding acquisition, J.B. and M.X.

Competing interests

The authors declare no competing interests.

Additional information

Supplementary information The online version contains supplementary material available at https://doi.org/10.1038/s41467-025-60374-4.

Correspondence and requests for materials should be addressed to Mingyi Xie.

Peer review information *Nature Communications* thanks the anonymous reviewers for their contribution to the peer review of this work. A peer review file is available.